



HAL
open science

γ' -V₂O₅ polymorph as a promising host structure for potassium storage: an electrochemical and structural study

Ankush Bhatia, Jean Pierre Pereira-Ramos, Nicolas Emery, Rita Baddour-Hadjean

► **To cite this version:**

Ankush Bhatia, Jean Pierre Pereira-Ramos, Nicolas Emery, Rita Baddour-Hadjean. γ' -V₂O₅ polymorph as a promising host structure for potassium storage: an electrochemical and structural study. *Chemistry of Materials*, inPress, 33 (13), pp.5276-5289. 10.1021/acs.chemmater.1c01390. hal-03280034

HAL Id: hal-03280034

<https://hal.science/hal-03280034>

Submitted on 7 Jul 2021

HAL is a multi-disciplinary open access archive for the deposit and dissemination of scientific research documents, whether they are published or not. The documents may come from teaching and research institutions in France or abroad, or from public or private research centers.

L'archive ouverte pluridisciplinaire **HAL**, est destinée au dépôt et à la diffusion de documents scientifiques de niveau recherche, publiés ou non, émanant des établissements d'enseignement et de recherche français ou étrangers, des laboratoires publics ou privés.

γ -V₂O₅ polymorph as a promising host structure for potassium storage: an electrochemical and structural study

Ankush Bhatia¹, Jean-Pierre Pereira-Ramos¹⁺, Nicolas Emery¹, Rita Baddour-Hadjean^{1*}

¹ Institut de Chimie et des Matériaux Paris Est (ICMPE), UMR 7182 CNRS-Université Paris Est Créteil, 2 rue Henri Dunant, 94320 Thiais, France

+ pereira@icmpe.cnrs.fr

* baddour@icmpe.cnrs.fr

ABSTRACT: K-ion batteries (KIBs) are receiving increasing interest because of the low K⁺/K redox potential and their reduced cost. This emerging alternative is however strongly dependent on the development of cathode materials with suitable structure for accommodating K⁺ ions. We show here the promising properties of the puckered layered γ -V₂O₅ polymorph that inserts up to 0.9 K⁺ mol⁻¹ at 3.3 V vs K⁺/K at C/60. An initial depotassiation capacity of 72 mAh g⁻¹ corresponding to the exchange of 0.5 K⁺ ions is still delivered at C/10 and a reversible capacity of 48 mAh g⁻¹, stable over 100 cycles, is achieved in the 4.4 V – 2.4 V voltage window. The reaction mechanism, investigated by XRD and Raman spectroscopy, involves the formation on first discharge of a new layered K_xV₂O₅ host structure. The K_{0.78}V₂O₅ bronze obtained at 2.4 V exhibits unfolded V₂O₅ sheets and an unexpected moderate expansion of the interlayer spacing compared to γ -V₂O₅. Depotassiation-potassiation reversibly occurs within K_xV₂O₅ (0.3 ≤ x ≤ 0.78) with less than 2% breathing. Such findings demonstrate the remarkable structural flexibility of γ -V₂O₅ to accommodate the large-sized K⁺ ions and illustrates the richness of V₂O₅ polymorphs as positive electrode materials for KIBs.

1. INTRODUCTION

The Li-ion battery (LIB) technology, firstly used in portable electronic devices, is now expanding to large scale applications like electric vehicles and stationary energy storage systems combined to the development of renewable energies. During the last decade, sodium-ion batteries (SIBs) have been extensively investigated as less expensive alternatives to LIBs, offering an appealing compromise between performance and cost [1]. More recently, potassium-ion batteries (KIBs) have emerged as additional interesting substitutes [2, 3] due to the lower redox potential of K⁺/K vs Na⁺/Na (-2.93 V vs -2.71 V/ENH) that has led to the identification of high operating voltage K-based materials [4–9]. An additional key advantage for obtaining high rate capability cathode and anode materials is provided by the lowest desolvation energy of K⁺ in various organic solvents compared to Li⁺ and Na⁺. Furthermore, the attractive electrochemical behavior of graphite as negative electrode has considerably boosted research efforts on high performance KIBs, even if numerous other anode materials have been further investigated like hard and soft carbon, porous carbon, intercalation anodes etc...[2, 3].

Although efforts to discover and develop new cathode materials for KIBs are in their infancy compared with those for anodes, the search of appropriate positive electrode materials is a crucial point for the successful development of KIBs. The major obstacle is the large ionic radius of K⁺ (1.38 Å) compared to Li⁺ (0.76 Å) or Na⁺ (1.02 Å), that limits the number of suitable host materials capable of accommodating K without large stresses or volume changes. In addition, repulsive K⁺–K⁺ coulombic interactions could limit transport properties in the crystal framework and then the rate capability. Looking back on the history of LIBs and NIBs, layered cobalt oxides P2- and P3-type K_xCoO₂ have been first considered, but they exhibit limited reversible capacities, multiple phase transitions and low operating potential [10,11]. Specific capacities between 90-120 mAh g⁻¹ have

been reported for Mn-based layered oxides, depending on the structure, the chemical composition and the voltage range [12–19]. In recent years, great research efforts have been made toward challenging Prussian blue KFe₂(CN)₆ [8], Prussian blue analogs [9] and polyanionic compounds AM_x(XO₄)_y, (X = P and S) which display robust 3D frameworks with large channels for ion storage and migration [2, 3]. Among them, V-based compounds such as KVP₂O₇, K₃V₂(PO₄)₃, K₃V₂(PO₄)₂F₃, KVPO₄F, and KVOPO₄ were found to exhibit a high operating voltage > 4 V vs. K⁺/K, much higher than the potentials observed for most of the K-based layered transition metal oxide materials, and capacities in the range 54 – 100 mAh g⁻¹ [3, 5]. However, less attention has been paid to layered V-based oxides offering also open structures suitable for K⁺ accommodation. Hydrated phases such as V₃O₇·H₂O [20] and V₂O₅·0.6-0.8H₂O [21, 22] have been considered with great interest. V₃O₇·H₂O displays a discharge capacity of about 150 mAh g⁻¹ at an average potential of 2.5 V vs. K⁺/K but 25% capacity loss after 100 cycles [20] while V₂O₅·0.6-0.8H₂O exhibits scattered capacity values in the range 60 – 220 mAh g⁻¹ at 2.1 V – 2.5 V vs. K⁺/K with a huge capacity fading upon cycling in carbonate-based electrolytes [21, 22]. Bilayered expanded structures such as the NH₄V₄O₁₀ bronze [23] and K-preintercalated K_{0.42}V₂O₅·0.25H₂O [24] were also reported, with the best capacity of 220 mAh g⁻¹ in the 4.3 V – 2 V window for the latter one, but 26% and 42% capacity loss after 50 cycles at C/15 and C, respectively [24]. In that case, the mechanism for discharge-charge process was reported as a genuine potassium intercalation reaction, which is questionable since 30% of the capacity was ascribed to non-faradaic contribution. Anhydrous potassium vanadium bronzes have been also considered as possible cathode materials for KIBs. The bilayered δ -K_{0.5}V₂O₅ phase [25, 26] have recently emerged as promising materials due to interesting capacity values, from 80 mAh g⁻¹ at room temperature in the 3.75 V – 1.5 V voltage range [25] to 130 mAh g⁻¹ at 35°C between 4.5 V and 2 V [26]. A layered K_{0.83}V₂O₅ bronze

with promising performance (80 mAh g⁻¹ in the 4.5 V – 1.5 V range) was also recently reported [27]. However, the discharge-charge behavior was carried out in highly concentrated 7 M KTFSI/ ethylene carbonate (EC): diethylene carbonate (DEC) electrolyte, which makes a straightforward comparison difficult.

Surprisingly, the layered α -V₂O₅ polymorph, among the first transition metal oxide identified as Li intercalation compound, has been little studied as potassium storage material. The pioneering work of one of us, 30 years ago, using a molten dimethylsulfone potassium electrolyte at 150°C, has proved the electroformation of orthorhombic K_xV₂O₅ bronze (0 < x < 0.6) with a structure closely related to that of the parent oxide [28]. However, potassium extraction was reported to be limited to 50%. Since then, only a few papers have focused on the K-storage properties of α -V₂O₅ at room temperature in usual organic based-electrolytes [29, 30]. Using a specific electrode design to improve the electronic conductivity and decrease the diffusion pathways, Atomic Layer Deposited core-shell structured amorphous α -V₂O₅@CNT (carbon nanotube) sponge showed a difficult reaction: the discharge profile spread over a wide potential range, with a low mid-discharge voltage of 1.75 V vs. K⁺/K and capacity values of 50 – 200 mAh g⁻¹, depending on the C rate [29]. In the wider 4.25 V – 1.5 V range, capacities of 200 mAh g⁻¹ were reported for crystalline α -V₂O₅ nanorods@rGO (reduced graphene oxide) heterostructure [30]. These recent results illustrate the modest performance of the orthorhombic α -V₂O₅ oxide that seems to be penalized by a low discharge potential, around 2 V vs. K⁺/K at best.

Another strategy than conventional carbon-based heterostructure must therefore be applied to face the challenge of an appropriate V₂O₅ host structure more favorable for K storage. Recent studies based on DFT calculations have outlined the interest of metastable V₂O₅ polymorphs obtained from topochemical removal of cations from the M_xV₂O₅ bronzes (M = Li, Cu, Ag) [31, 32]. Lower diffusion barriers and higher operating voltage are predicted for such cation-free metastable phases. As a proof of concept, our group has demonstrated the attractive features of the γ -V₂O₅ polymorph, that is the charge product of the γ -LiV₂O₅ phase formed upon electrochemical lithiation of α -V₂O₅ at 2.3 V vs. Li⁺/Li [33]. γ -V₂O₅ exhibits the same orthorhombic symmetry than α -V₂O₅, but benefits however from a larger interlayer spacing of \approx 5 Å (vs. 4.37 Å for α -V₂O₅) as well as a corrugated structure enabling superior electrochemical performance toward Li⁺ [34, 35] and Na⁺ [36–39] insertion compared to α -V₂O₅ [40, 41]. Indeed, γ -V₂O₅ is able to accommodate almost 1 Na⁺ mol⁻¹ of oxide (145 mAh g⁻¹), remarkably at the same working voltage than Li⁺ (3.3 V vs Na⁺/Na).

Hence, stimulated by the appealing sodiation properties of the layered puckered γ -V₂O₅ oxide and the need for new cathode materials for KIBs, we investigate here for the first time the electrochemical properties of this polymorph at room temperature in a potassium-metal cell. We provide also a detailed picture of the K-storage mechanism in γ -V₂O₅ during the discharge-charge cycle through *ex-situ* X-ray diffraction (XRD) and Raman spectroscopy. The electrochemical formation on first discharge of a new layered K_xV₂O₅ structure (0.5 ≤ x ≤ 0.78) showing reversible K⁺ insertion-extraction properties in the 4.4 V – 2.4 V voltage range is demonstrated. The peculiar

structural features of this electroformed potassium vanadium bronze are described in details. They highlight the interest of the puckered layered γ -V₂O₅ polymorph to accommodate the expected large deformation upon electrochemical K incorporation.

2. EXPERIMENTAL PROCEDURE

2.1. Synthesis. γ -V₂O₅ was obtained by chemical oxidation of γ -LiV₂O₅ synthesized from the chemical lithiation of α -V₂O₅ precursor. This precursor was prepared under mild-temperature conditions according to the polyol method [42] whose characteristic is to lead to very fine powder with a narrow and homogeneous particle size distribution. By reaction with an excess of lithium iodide in acetonitrile, the intermediate δ -LiV₂O₅ phase is formed. After washing in acetonitrile and drying at 70 °C, the obtained powder was heat treated at 300°C for 2 hours under dynamic primary vacuum in a Büchi® furnace to allow the phase transition towards γ -LiV₂O₅. Li extraction from γ -LiV₂O₅ was performed by reacting 500 mg of the bronze in a NO₂BF₄ solution (solid Alfa Aesar, 96%) in acetonitrile (V₂O₅/NO₂BF₄, molar ratio 1/2) under stirring for 1h at room temperature. These experimental conditions ensure the quantitative Li deintercalation from the γ -LiV₂O₅ precursor. After reaction and decantation, the supernatant liquid was removed by pipetting. Powder was washed three times with acetonitrile and then vacuum dried at 70°C for 12h. The powder color changes from black to orange, which indicates the loss of metallic properties, thus confirming the complete lithium deintercalation. Electrochemical titration using galvanostatic oxidation and chemical redox titration confirmed the +5 oxidation state of vanadium in γ -V₂O₅.

2.2. Characterization techniques. The pristine powder and the electrodes were characterized by scanning electron microscopy (SEM), Zeiss, Merlin-type microscope. Elemental composition were determined from Electron Dispersive X-ray Spectroscopy (EDS) analysis together with SEM using an accelerating voltage of 10 – 15 kV. Crystal structures were investigated using XRD and Raman spectroscopy. XRD experiments were performed using a Panalytical XPert pro apparatus equipped with a X'Celerator detector and using Co K α radiation (λ K α = 1.789 Å). The as-collected patterns have been analyzed using Rietveld refinement method with the GSAS ExpGUI package [43, 44]. The graphite contribution has been included with a correction of the preferential orientation (*00l* reflection intensities are exacerbated due to the preparation process of the electrode). A small excluded region was added to avoid possible contribution of the PTFE binder (one single peak at 21°). Raman spectra were recorded with a LaBRAM HR 800 (Jobin-Yvon, Horiba) Raman micro-spectrometer including Edge filters and equipped for signal detection with a back illuminated charge coupled device detector (Spex CCD) cooled by Peltier effect to 200 K. A He:Ne laser (632.8 nm) was used as the excitation source. The spectra were measured in back-scattering geometry. To avoid local heating of the sample, the power of the laser beam was adjusted to 0.2 – 0.5 mW with neutral filters of various optical densities. The resolution was about 0.5 cm⁻¹. A 100× objective was used to focus the laser light on sample surface to a spot size of 1 μ m².

2.3. Electrochemical experiments. The positive electrode was prepared by mixing 80 wt% of active material with 7.5 wt % of acetylene black, 7.5 wt % of graphite and 5 wt% of PTFE as binder. About 6 mg of this mix was directly deposited on the coin cell current collector.

CR2032 coin-cells were assembled in argon-filled glovebox where water and oxygen concentrations were kept less than 1 ppm. The coin cells were filled with and contain potassium metal as negative electrode. The positive electrode was separated from the negative electrode by Whatman glass fiber disks soaked by the electrolyte 0.5 M KPF₆ (EC): propylene carbonate (PC) 1:1 electrolyte, 2% vol. fluoroethylene carbonate (FEC). Electrochemical experiments were carried out at 20°C using a VMP3 Biologic apparatus, in the 4.4 V – 2.4 V and 4.4 V – 1.5 V voltage ranges.

The structural investigation was carried out in the 4.4 V – 2.4 V potential window by using two electrodes coin cells. The cells were discharged (and charged) at C/20 rate (7 mA g⁻¹) up to the required x composition in K_xV₂O₅ (0 ≤ x ≤ 0.78). The cells were then disassembled in the glove box. The positive electrodes were rinsed 3 times with DMC in order to remove any electrolyte residues and placed in appropriate airtight sample holders to be further analyzed by XRD and Raman spectroscopy. Raman spectra were systematically recorded on 10 different spots of each electrode. Very similar spectra were obtained whatever the illuminated spot, indicating a homogeneous potassiumation/depotassiation reaction in the chosen experimental conditions.

3. RESULTS AND DISCUSSION

3.1. Structural characterization of γ' -V₂O₅. As shown in **Figure 1**, the pristine γ' -V₂O₅ powder is homogeneous, made of small platelets of 500 nm long maximum and ~ 200 nm wide. This results from the solution technique used to synthesize the γ' -phase. The XRD pattern of γ' -V₂O₅ as-prepared powder (**Figure 2a**) is fully indexed using an orthorhombic symmetry (*Pnma* space group). The Rietveld refinement (**Figure S1**) indicates the presence of a pure and well crystallized γ' -V₂O₅ phase, with unit cell parameters *a* = 9.95 Å, *b* = 3.59 Å, *c* = 10.04 Å, in good agreement with previous data [34, 36]. γ' -V₂O₅ has a layered structure composed of infinite ribbons parallel to the *b* axis made of edges-sharing VO₅ distorted pyramids oriented alternatively up and down, which leads to two non-equivalent vanadium environments (see inset of **Figure 2a**). These ribbons are linked to each other along the *a*-direction by one pyramid corner oxygen forming puckered layers perpendicular to the *c*-axis. The mean crystallite size estimated from diffraction peaks width is 50–60 nm.

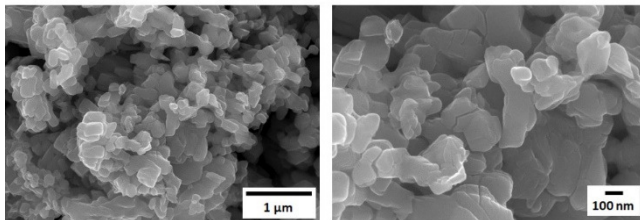


Figure 1. SEM micrographs of as-prepared γ' -V₂O₅ powder

The Raman spectrum of γ' -V₂O₅ is displayed in **Figure 2b**. The projection of the γ' -V₂O₅ structure along the *b*-crystallographic direction showing all the V–O contacts in the two vanadium environments (V_a, V_b) is shown in inset of **Figure 2b**. This Raman fingerprint is characteristics of the γ' -V₂O₅ polymorph, as previously reported in details [45, 46]. The whole vibrations of the chains can be identified: the highest frequency peaks in the 990–1050 cm⁻¹ region correspond to the stretching modes of the shortest apical V=O₁ bonds, named *v*(V=O₁). There are eight vanadyl bonds in the unit cell of the γ' -structure (see inset in **Figure 2b**), and therefore there are eight *v*(V=O₁) modes from which four are Raman active [46]. One of them involve the in-phase oscillations of all vanadyl bonds, and this mode is the very high Raman band observed at 1003 cm⁻¹. Next in frequency, bands at 752 and 603 cm⁻¹ are related to the asymmetric and symmetric bond stretching vibrations localized within the V_a–O₃–V_b bridges, respectively. The stretching modes of the V_a–O_{2a}–V_a and V_b–O_{2b}–V_b bridges forming the rails of the ladders are observed at 722 and 694 cm⁻¹. Modes involving the V_a–O_{2a} and V_b–O_{2b} ladder step bonds (indicated by dashed line) are seen at 532 and 500 cm⁻¹. Bands at 138, 171, 190, 238, 266, 282, 299, 349 and 390 cm⁻¹ are assigned to the complex distortions of the V₂O₅ ladders while the two lower frequency modes at 92, 126 and 153 cm⁻¹ correspond to the rotational motions of the two vanadium atoms [45, 46].

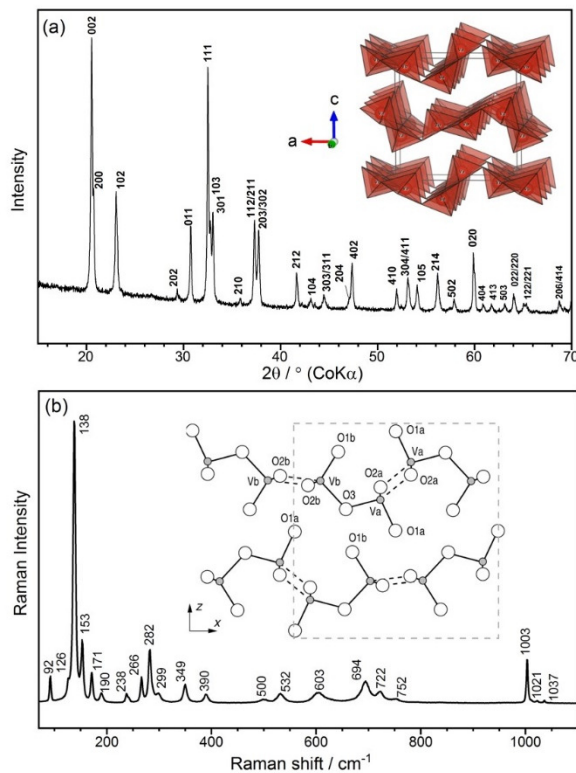


Figure 2. (a) X-ray diffraction pattern of γ' -V₂O₅ Inset: crystal structure of γ' -V₂O₅ (b) Raman spectrum of γ' -V₂O₅. Inset: projection of the structure of γ' -V₂O₅ along the *b*-crystallographic direction showing all the V–O contacts. Dashed lines show V–O inter-chain ladder-step bonds. The dashed light blue rectangle indicates the unit cell.

3.2. Electrochemical study. The first discharge-charge cycle of γ' -V₂O₅ at 20°C at C/20 rate (7 mA g⁻¹) in the two 4.4 V – 2.4 V (**Figure 3a**) and 4.4 V – 1.5 V (**Figure 3b**) regions show one-step profile consisting mainly in a flat voltage plateau at high potential of 3.3 V vs K⁺/K. The faradaic yield increases from 0.78 to 0.87 F mol⁻¹ of oxide when lowering the cutoff voltage from 2.4 to 1.5 V, while the first charge efficiency of 64% suggests that 0.3 K⁺ are irreversibly trapped in the discharged product. The remaining exchanged 0.5 to 0.56 K⁺ ions lead to a reversible capacity of 72–82 mAh g⁻¹. The large hysteresis of about 600 mV between discharge and charge reveals a difficult oxidation. A limited charge efficiency of 66% was also previously reported for layered δ -K_{0.5}V₂O₅, even under GITT conditions [25]. It is worth noting the present discharge-charge profile showing one single step strongly resembles that reported for electrochemical Li and Na insertion in γ' -V₂O₅ [34–38]. Such similarity suggests potassium insertion also takes place in γ' -V₂O₅, leading to K_xV₂O₅ bronzes ($x = 0.78$ or 0.87), depending on the cutoff voltage (2.4 V or 1.5 V, respectively).

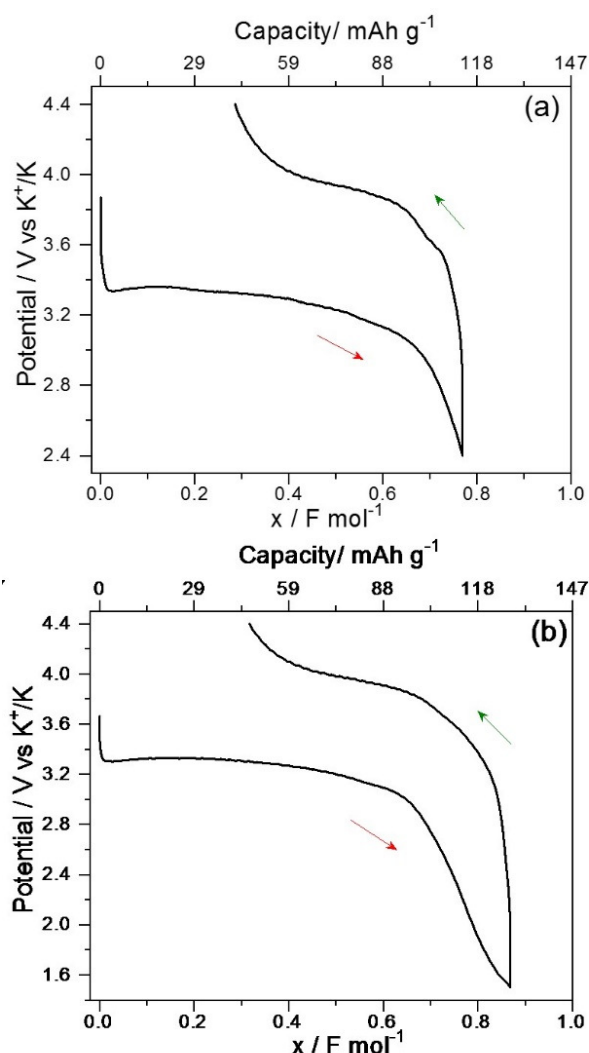


Figure 3. First discharge-charge cycle at 20°C of γ' -V₂O₅ in the (a) 4.4 V – 2.4 V; (b) 4.4 V – 1.5 V voltage windows. C/20 rate; Electrolyte 0.5 M KPF₆/EC: PC 1:1; 2% vol. FEC.

In spite of the larger size of potassium, the mean discharge potential of 3.3 V vs K⁺/K (≈ 3.1 vs Na⁺/Na), is lower by only ≈ 200 mV than that observed for lithiation and sodiation.

This moderate voltage lowering demonstrates the appealing properties of the flexible puckered structure of γ' -V₂O₅ that is able to accommodate nearly the same molar amount of Li⁺ (1), Na⁺ (0.96) and K⁺ (0.87) ions at a potential above 3 V, following the sequence $E(\text{Li}) \approx E(\text{Na}) > E(\text{K})$. The slightly lower K content results from its larger ionic size and lower diffusivity. Finally, the most distinctive feature between K⁺ and Na⁺/Li⁺ accommodation lies in the lower charge efficiency for potassium while quantitative Li and Na extraction are achieved in the same experimental conditions (**Figure S2**) [34]. The high discharge potential of 3.3 V vs. K⁺/K for γ' -V₂O₅ combined with a single step process represent a tremendous asset in comparison with layered δ -K_{0.5}V₂O₅ [25, 26] showing two or three discharge steps at similar or lower mid-discharge voltages (3.2 V or 2.5 V).

In order to evidence probable kinetic limitations, the discharge-charge has been performed at lower rate of C/60 at 20°C (**Figure S3a**) and at C/60 at 50°C (**Figure S3b**). Once again, the potassium reaction in γ' -V₂O₅ proceeds along a high potential plateau located at 3.3/3.4 V vs K⁺/K. At 20°C, the potassium uptake increases from 0.78 to 0.90 from C/10 to C/60 and the charge efficiency increases, passing from 65% at C/10 to 71% at C/60. At 50°C, the oxidation reaction turns to be quasi-quantitative, even if some concomitant electrolyte decomposition seems to be promoted at 50°C above 3.8 V. Another noticeable feature is the discharge-charge hysteresis that lessens by a factor 2 (≈ 200 mV). These observations ascertain the sluggish diffusivity of K⁺ ions in the layered vanadium oxide.

Cycling performance of γ' -V₂O₅ has been examined at C/10 rate (15 mA g⁻¹) in the 4.4 V – 2.4 V potential window (**Figures 4a-b**). The capacity of 60 mAh g⁻¹ available after the second discharge decreases upon the following ten cycles, then a stable value of 48 mAh g⁻¹ is retained over at least 100 cycles. The coulombic efficiency of 100% from the second cycle indicates that no side reaction occurs in the 4.4 V – 2.4 V potential window. Rate capability tests shown in **Figure 4c** account for a moderately sluggish diffusion of potassium ions into γ' -V₂O₅. Indeed, the capacity decreases from 70 mAh g⁻¹ at C/20 (7 mA g⁻¹) to 51 mAh g⁻¹ at C/10 (15 mA g⁻¹), 40 mAh g⁻¹ at C/5 (29 mA g⁻¹) but still 37 mAh g⁻¹ at C (145 mA g⁻¹) and even 2C (290 mA g⁻¹). A capacity of 64 mAh g⁻¹, close to the initial one, can be recovered at C/20, suggesting the host lattice is not damaged after applying high 2C rate. The use of the enlarged 4.4 V – 1.5 V potential window turns to be detrimental to the capacity retention (**Figure S4**). Indeed, the initial capacity of 66 mAh g⁻¹ decreases rapidly to 50 mAh g⁻¹ over 20 cycles and then declines more slowly but continuously to reach 35 mAh g⁻¹ after 100 cycles.

The electrochemical behaviour at room temperature of the conventional α -V₂O₅ polymorph has been also investigated for comparison. **Figure S5** shows the discharge-charge curves of a composite electrode obtained at C/20 in the same KPF₆/EC:PC electrolyte. In that case, the first reduction exhibits a quasi-voltage plateau at much lower potential of 1.5 V, indicating the potassium reaction is much more difficult in α -V₂O₅ (**Figure**

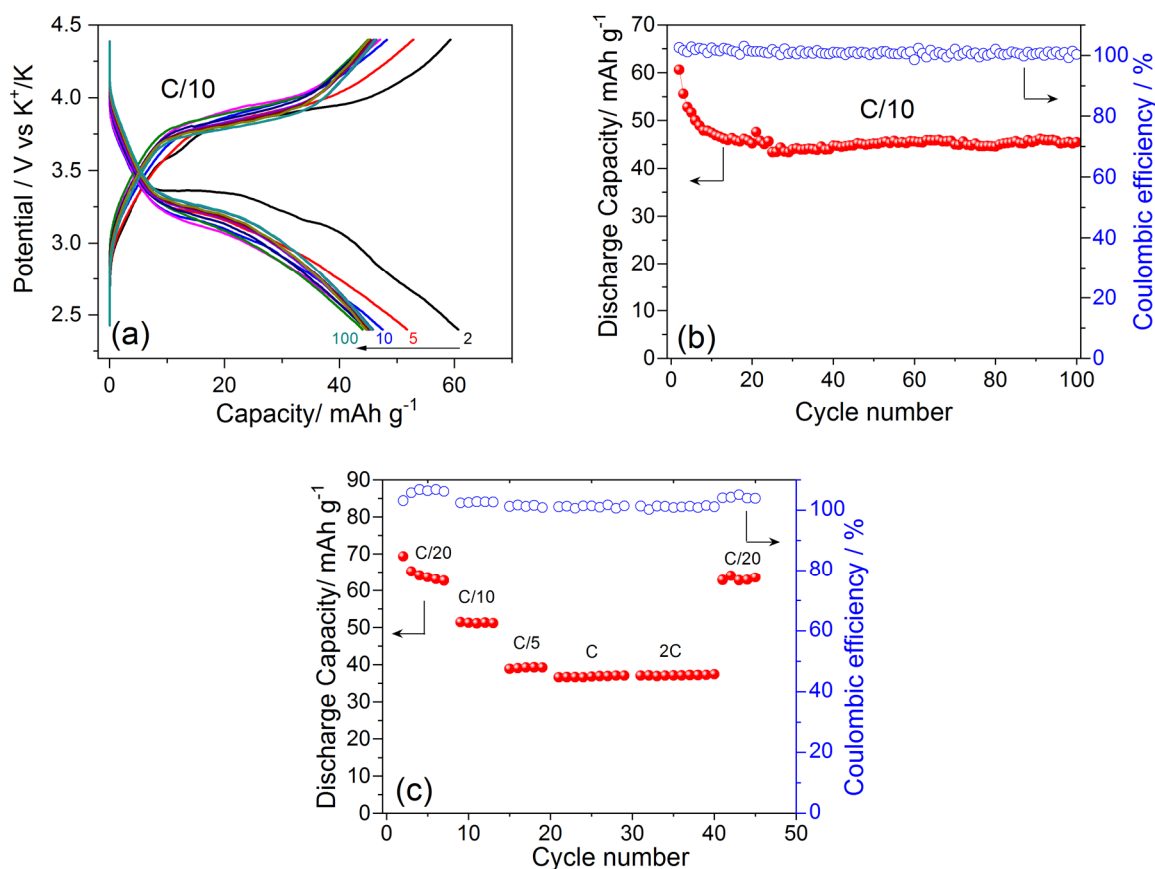


Figure 4. (a) Discharge-charge cycles of γ' - V_2O_5 at C/10 rate (b) Evolution of the specific capacity with cycles at C/10 rate; (c) Rate capability study. 4.4 V – 2.4 V voltage window. Electrolyte 0.5 M KPF₆/EC: PC 1:1; 2% vol. FEC.

S5a). Further cycles show sloping potential-composition dependence with a huge hysteresis (2.5 V) and a fast capacity decline leading to an available capacity of 40 mAh g⁻¹ after 50 cycles (**Figure S5b**). These results confirm the remarkable suitability of the γ' - V_2O_5 structure to accommodate K⁺ ions at a high energy level (3.3 V vs. K/K⁺), i.e. 1.8 V higher than the conventional α -polymorph, the corrugated nature of the sheets combined with a larger interlayer spacing providing probably more flexibility upon potassium insertion.

Comparison of γ' - V_2O_5 cycling properties with other V_2O_5 -based cathode materials for KIBs is a difficult task due to the use of various electrode technologies, electrolyte composition, cycling limits, current densities. In addition, most of candidates reported in literature are hydrated compounds such as V₃O₇·H₂O [20], V₂O₅·0.6H₂O [21, 22], (NH₄)_{0.5}V₂O₅·1.1H₂O [23], K_{0.42}V₂O₅·0.25H₂O [24], all characterized by a much lower working voltage around \approx 2.5 V and a significant capacitive contribution. Much interest is provided by the anhydrous bilayered δ -K_{0.5}V₂O₅ structure [25, 26], but contradictory properties and scattered cycling performances are reported. For instance, three main discharge steps (4.0 V, 3.1 V and 2.5 V) allow reaching a reversible capacity of 120 mAh g⁻¹ [26] while a two steps mechanism (3 V, 2.75 V) involving a lower capacity of 80 mAh g⁻¹ is described in [25]. The capacity systematically declines with cycles, by 12% at \approx C/10 to reach

70 mAh g⁻¹ in the 3.75 V – 1.5 V window [25] or by 33% after 100 cycles at C/3 between 4.5 V – 2 V to reach 80 mAh g⁻¹ [26]. However, in the latter case, electrochemical tests were performed at 35°C, using a high carbon loading (30 wt%). The mean operating potential upon cycling (\approx 3.1 V) observed here for γ' - V_2O_5 competes with that achieved for δ -K_{0.5}V₂O₅ nanobelts [25, 26]. Finally, an excellent capacity retention is the main distinctive feature of γ' - V_2O_5 since after 10 cycles, the available capacity of 48 mAh g⁻¹ is retained over at least 100 cycles at C/10, showing the structural stability of the electroformed potassium bronze. A nanosizing strategy applied to the γ' - V_2O_5 synthesis, combined with an appropriate electrode technology should allow to improve the charge efficiency and potassium diffusion in order to benefit from a better rate capability and cycle life. It is also worth mentioning the performance of some vanadium-based polyanionic materials that have been developed for KIBs. KVPO₄F is reported to deliver at c.a. 4.3 V a promising capacity of about 90 mAh g⁻¹ involving four successive phase transitions [2, 3]. However, a significant 30–40% capacity loss upon cycling was attributed to electrolyte decomposition [47]. Furthermore, the NASICON-type K₃V₂(PO₄)₃/C nanocomposite could deliver a charge capacity of \approx 77 mAh g⁻¹ and a discharge capacity of \approx 54 mAh g⁻¹ [48] while a recent study demonstrates that

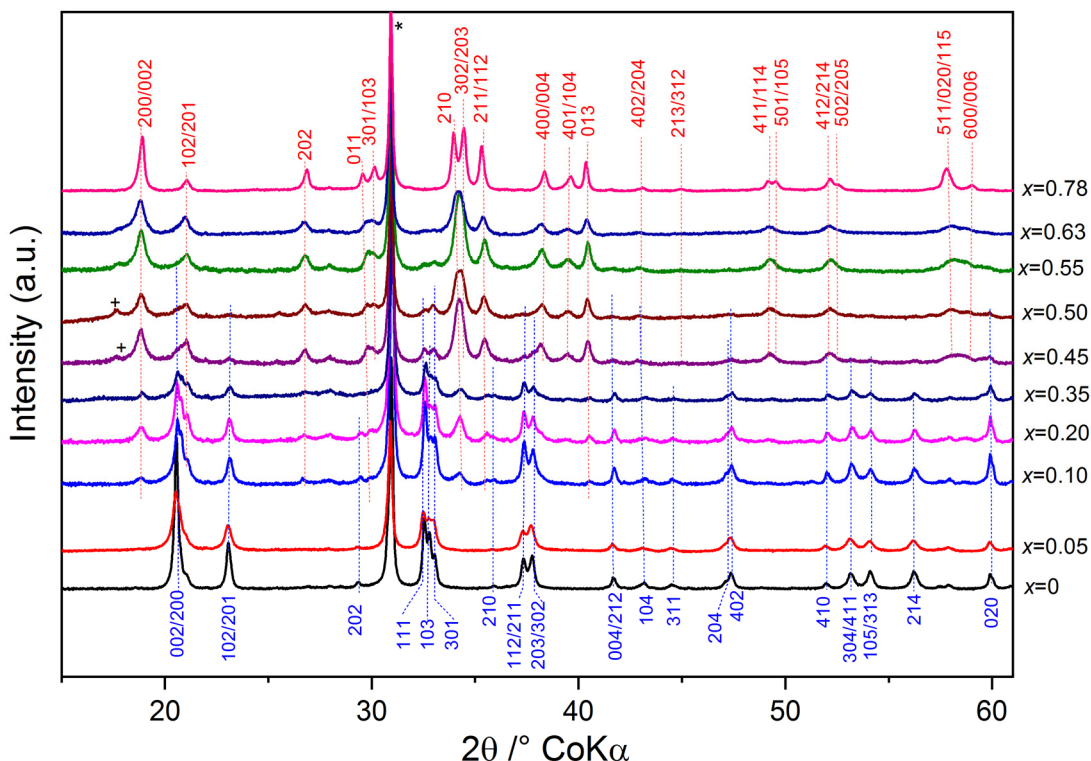


Figure 5. X-ray diffraction patterns of reduced γ' - V_2O_5 electrodes during the first discharge at C/20 as a function of the faradaic yield x ($F \text{ mol}^{-1}$). $0 \leq x \leq 0.78$ (4.4 V – 2.4 V voltage window). *: Graphite reflection.

$K_3V_2(PO_4)_2F_3$ could exhibit a specific capacity of 100 mAh g^{-1} at an average voltage of 3.7 V [49].

Very recently, a $K_{0.83}V_2O_5$ bronze has been chemically prepared [27], according to a solution technique adapted from that reported by Emery et al. for preparing the sodiated γ - $Na_{0.96}V_2O_5$ bronze with orthorhombic symmetry ($Pnma$ space group) and lattice parameters $a = 10.95 \text{ \AA}$, $b = 3.73 \text{ \AA}$ and $c = 10.93 \text{ \AA}$ [39]. The electrochemical properties of the chemically prepared $K_{0.83}V_2O_5$ were studied in not prevalent practical conditions, i.e. using a highly concentrated electrolyte (7 M KTFSI/ EC:DEC). After an initial charge process allowing 0.68 K^+ ion to be removed from the structure, a stable capacity near 80 mAh g^{-1} was achieved upon cycling at C/15, however spread over the broad 4.3 V – 1.5 V potential window. This capacity value is higher than that obtained in the present study performed in usual 0.5 M KPF₆/ EC:PC electrolyte but the mid-discharge voltage is lower, only 2.75 V against 3.1 V here.

EDS data achieved on electrodes discharged at C/20 at 2.4 V and 1.5 V, as well their charged product, are gathered in **Table 1**. A satisfactory agreement is found between the K/V ratios obtained from EDS measurements and the faradaic yields drawn from galvanostatic curves (**Figures 3a-b**). This analysis confirms potassium ions actually incorporate the γ' - V_2O_5 cathodic material upon discharge and are removed upon charge. Nevertheless, as shown in **Table 1**, the charge process does not allow the complete removal of potassium bronze, and leads to the $K_{\approx 0.3}V_2O_5$ compound, whatever the voltage window.

3.3. Structural mechanism in the 4.4 V – 2.4 V potential range.

To grasp insights into the structural modifications associated to electrochemical K insertion in γ' - V_2O_5 , XRD and Raman spectroscopy experiments have been performed during the first discharge ($0 \leq x \leq 0.78 \text{ F mol}^{-1}$) and further cycles in the 4.4 – 2.4 V potential range.

3.3.1. Study of the first discharge. The XRD patterns of reduced electrodes as a function of the faradaic yield x (in $F \text{ mol}^{-1}$), $0 \leq x \leq 0.78$, are reported in **Figure 5**. For $x = 0.05$, no change is observed in the XRD pattern, showing $K_{0.05}V_2O_5$ exhibits the same cell parameters than the pristine γ' - V_2O_5 electrode ($a = 9.95 \text{ \AA}$, $b = 3.59 \text{ \AA}$ and $c = 10.04 \text{ \AA}$). The first indicators of structural evolution upon reduction appear from $x = 0.1$, through the presence of a new set of reflection lines (see red dotted lines), the main ones being located at 18.85° , 26.8° , 34.2° , 35.45° and 40.5° . In the $0.1 \leq x \leq 0.5$ composition range, this additional set of peaks grows at the expense of the γ' - V_2O_5 reflections (see blue dotted lines), which is indicative of a biphasic region where the pristine oxide and a new $K_xV_2O_5$ phase coexist. For $x = 0.45$ and 0.50 , the presence of a low intensity line located at 17.6° (labelled as + in **Figure 5**) could indicate the formation of an intermediate phase with γ -type structure showing a complex potassium filling scheme of the interlayer spacing within the b direction (see **Figure S6**). Due to the size of K^+ ions and the shape of the possible crystallographic sites available for the alkaline species, a distribution of K^+ on half of the sites would explain the doubling of b parameter. For $0.5 <$

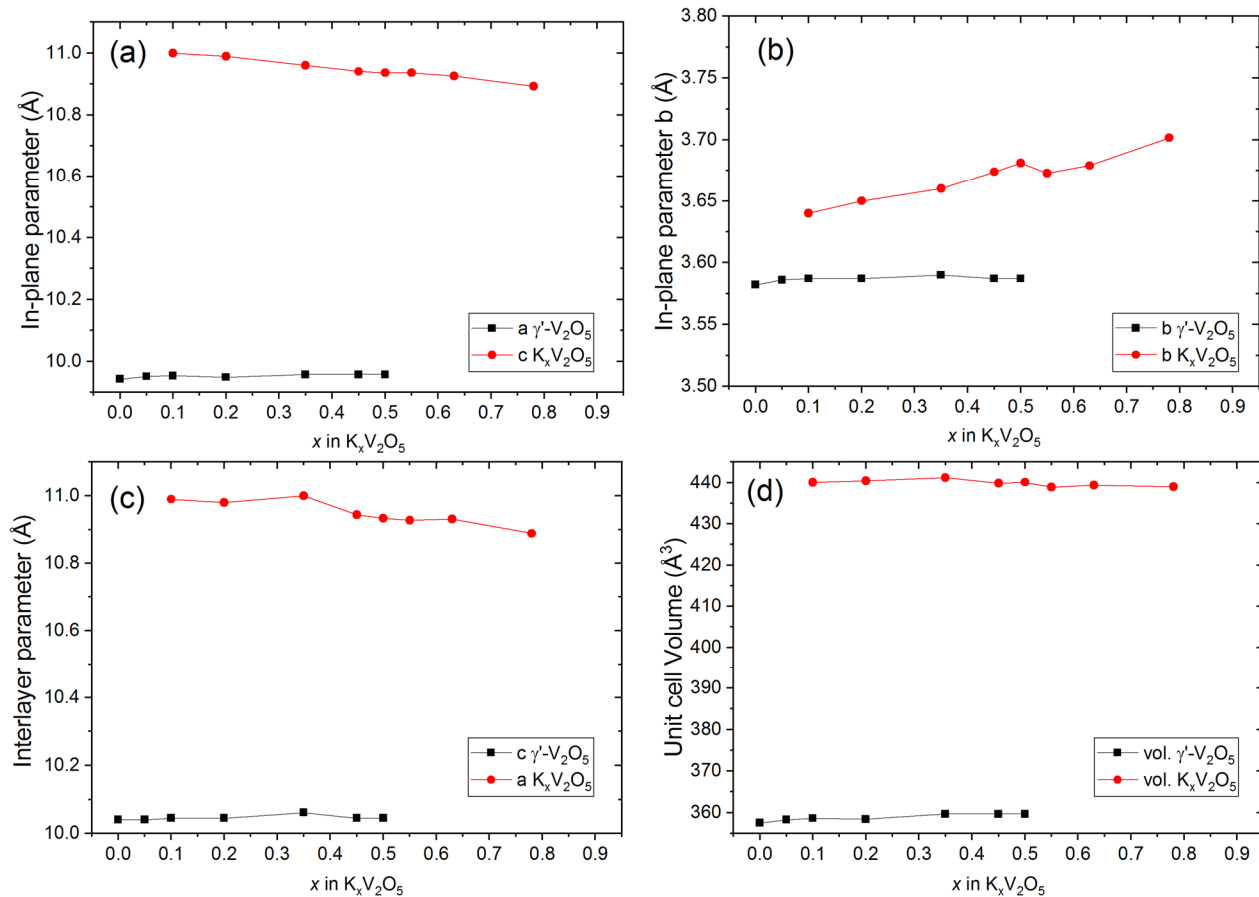


Figure 6. Evolution of the unit cell parameters a , b , c and unit cell volume V of reduced γ '- V_2O_5 electrodes during the first discharge at $C/20$ as a function of the faradaic yield x (F mol^{-1}). $0 \leq x \leq 0.78$ (4.4 V – 2.4 V voltage window). Black squares: K-poor γ - $\text{K}_x\text{V}_2\text{O}_5$; Red circles: K-rich $\text{K}_x\text{V}_2\text{O}_5$ phase.

$x \leq 0.78$, a pure solid solution of $\text{K}_x\text{V}_2\text{O}_5$ is evidenced, characterized by 19 reflections in the 15 – 60° 2θ range (see red-labelled peaks). The $\text{K}_x\text{V}_2\text{O}_5$ potassium-containing phase ($0.5 \leq x \leq 0.78$) has been indexed using an orthorhombic cell, within the same space group as γ '- V_2O_5 , i.e. $Pnma$. Note that the symmetry elements of this phase in the $Pnma$ space group imply an inversion between a and c parameters as compared to γ '- V_2O_5 , the interlayer distance in $\text{K}_x\text{V}_2\text{O}_5$ ($0.5 \leq x \leq 0.78$) being related to the a parameter while the c parameter corresponds to one of the two in-plane distances.

In summary, this XRD study shows the existence of three main domains during the discharge of γ '- V_2O_5 : (i) a narrow solid solution region of γ - $\text{K}_x\text{V}_2\text{O}_5$ for $0 \leq x \leq 0.05$ at the beginning of the discharge; (ii) A wide two-phase domain for $0.05 < x \leq 0.5$ along the quasi-voltage plateau at 3.3, where γ - $\text{K}_{0.05}\text{V}_2\text{O}_5$ and a new $\text{K}_{0.5}\text{V}_2\text{O}_5$ phase coexist; (iii) A solid solution composition region ($0.5 < x \leq 0.78$) at the end of the discharge, where $\text{K}_{0.5}\text{V}_2\text{O}_5$ becomes enriched up to $\text{K}_{0.78}\text{V}_2\text{O}_5$.

The detailed evolution of the lattice parameters and volume of K-poor " γ - $\text{K}_x\text{V}_2\text{O}_5$ " and K-rich $\text{K}_x\text{V}_2\text{O}_5$ phases as a function of x ($0 \leq x \leq 0.78$) is shown in **Figure 6**. It is clear then that the very first potassium ions ($0 < x \leq 0.05$) can be accommodated

in γ '- V_2O_5 without modifying its unit cell parameters. However, from $x = 0.1$, the new K-rich $\text{K}_x\text{V}_2\text{O}_5$ phase growing at the expense of the K-poor " γ - $\text{K}_x\text{V}_2\text{O}_5$ " exhibits significantly increased lattice parameters values: the in-plane a parameter expands by 10.5% (from 9.95 Å to 11.00 Å, see **Figure 6a**); the interlayer parameter also increases in the same order of magnitude (from 10.04 to 10.98 Å, +9.4%, see **Figure 6c**). A less moderate variation occurs for the in-plane b parameter (+1.7%, see **Figure 6b**), suggesting potassium diffusion takes place along the b direction, as reported for lithiation and sodiation [34, 36]. Within the biphasic domain ($0.1 \leq x \leq 0.5$), slight evolutions take place within the potassiated system: a (-0.6%), b (+1%) and c (-0.5%). The same trend is observed in the solid solution domain of the potassium-rich $\text{K}_x\text{V}_2\text{O}_5$ phase ($0.50 < x \leq 0.78$). The unit cell parameters of the fully discharged $\text{K}_{0.78}\text{V}_2\text{O}_5$ phase are $a = 10.89$ Å, $b = 3.70$ Å and $c = 10.89$ Å.

The present structural findings call for specific comments when compared with previous data achieved in the case of electrochemical lithiation and sodiation of γ '- V_2O_5 (see **Table 2**). Owing to the bigger Shannon's ionic radius of K^+ ions as compared to Na^+ and Li^+ (1.38 Å $>$ 1.02 Å $>$ 0.76 Å, respectively [50]), one should expect a greater interlayer increase upon K accommodation. However, as seen in **Table 2**, while 6% and

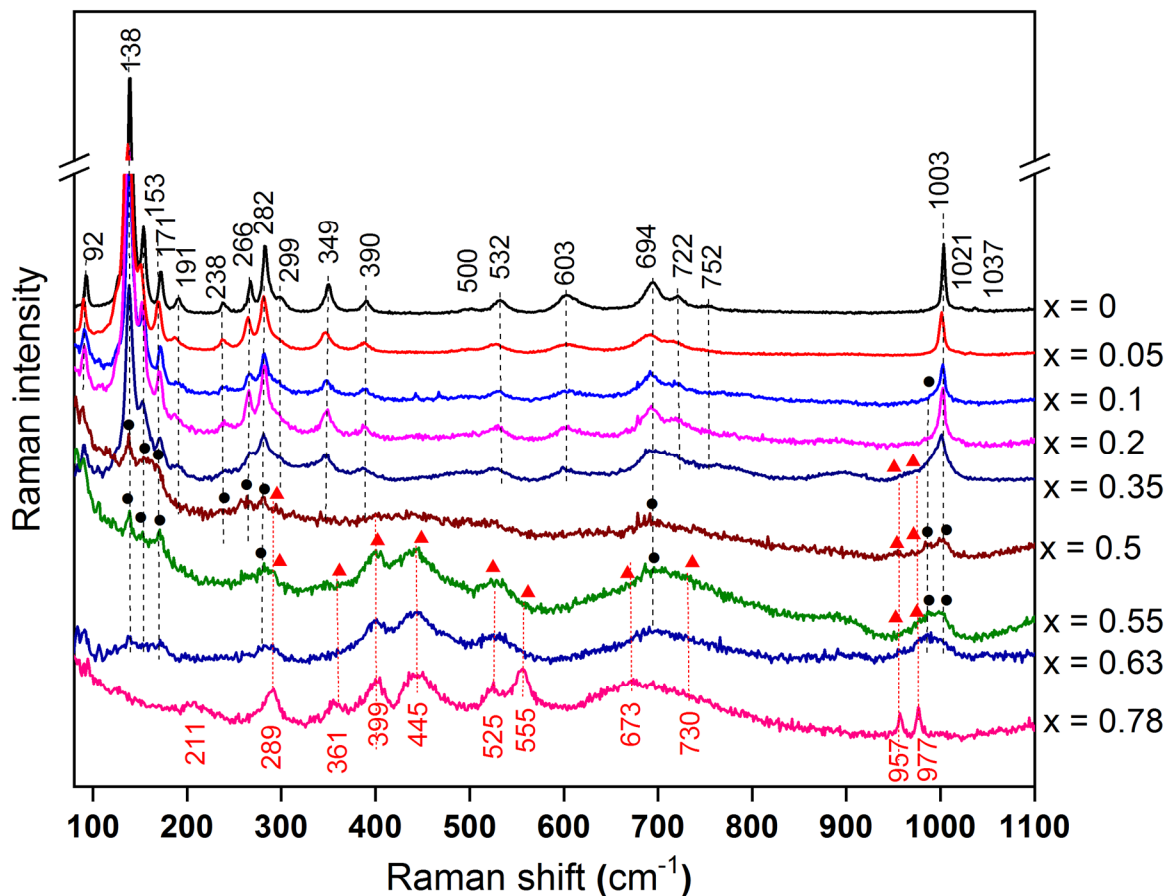


Figure 7. Raman spectra of reduced γ' - V_2O_5 electrodes during the first discharge at C/20 as a function of the faradaic yield x ($F \text{ mol}^{-1}$), $0 \leq x \leq 0.78$ (4.4 V – 2.4 V voltage window). Black spheres: K-poor γ - $K_xV_2O_5$; Red triangles: K-rich $K_xV_2O_5$ phase.

18% interlayer parameter expansion occurs upon Li [34] and Na [36] insertion, respectively, an increase by only 8.5% is observed here upon potassiation. This limited interlayer expansion can be understood at the light of the much higher polarizability of K^+ ion [51], allowing it to distort much more. Another peculiar feature of potassium accommodation in the γ' - V_2O_5 lattice is the significant unpuckering of the V_2O_5 layers, as revealed by the 9.4% increase in the in-plane parameter (see **Table 2** and **Figure 6a**).

It is noteworthy a reverse trend was reported for lithiation and sodiation of γ' - V_2O_5 [34, 36], i. e. a contraction of the in-plane parameter of 2.6 % and 1.7 %, respectively, indicating a moderate puckering of V_2O_5 layers (see **Table 2**). This leads to a unit cell volume of $K_{0.78}V_2O_5$ larger than γ' - V_2O_5 by 22.6%, as compared to +4% and +18% for the lithiated and sodiated products, respectively (see **Figure 6d** and **Table 2**). The associate molar volume reaches $66 \text{ cm}^3 \text{ mol}^{-1}$. As a comparison, γ - $Na_{0.96}V_2O_5$ [36, 39] and α' - NaV_2O_5 [52] polymorphs exhibit lower molar volumes of 63 and $59 \text{ cm}^3 \text{ mol}^{-1}$, respectively, in accordance with the lower ionic radii of Na^+ than K^+ [50].

The Raman spectra of reduced electrodes as a function of the faradaic yield x , $0 \leq x \leq 0.78$, are shown in **Figure 7**. For $x = 0.05$, no change is observed in the Raman spectrum, showing $K_{0.05}V_2O_5$ is very close to the pristine γ' - V_2O_5 at the scale of the

chemical bond. For $0.1 \leq x \leq 0.35$, although the overall signature of γ' - V_2O_5 is kept, one can notice several progressive changes affecting the bands width and intensities. This band broadening and relative intensity decrease (especially that of the 138 cm^{-1} band) indicate the occurrence of some local disorder in the K-poor γ - $K_xV_2O_5$ upon potassium insertion. For $x = 0.1$, one new component at 986 cm^{-1} (indicated by a black sphere) can be detected at the bottom of the 1003 cm^{-1} band, which points to the partial reduction of the V^{5+} into V^{4+} ions within the γ - $K_xV_2O_5$ lattice. For $x = 0.35$, two new bands at 957 and 977 cm^{-1} (indicated by red triangles) point to the emergence of a new system coexisting with K-poor γ - $K_xV_2O_5$. For $x = 0.5$, the Raman signature of γ - $K_xV_2O_5$ is severely affected, showing a collapse of most of the bands (indicated by black spheres) while the new system manifests itself by three low components at 289 , 957 and 977 cm^{-1} (indicated by red triangles). Upon potassium enrichment in the $0.55 \leq x \leq 0.78$ composition range, the Raman spectrum of the new potassiated phase shows increasing additional features. For $x = 0.55$, the K-rich phase manifests itself through the rising of supplementary components at 361 , 399 , 445 , 525 , 555 , 673 and 730 cm^{-1} , in addition to the 289 , 957 and 977 cm^{-1} modes (see red triangles). One can still detect for $x = 0.55$ and $x = 0.63$ the residual presence of the K-poor γ - $K_xV_2O_5$ phase through the persistence of low intensity bands (indicated by black spheres) at 138 , 153 , 171 , 282 , 694 , 986 and 1003 cm^{-1} .

¹. For $x = 0.78$, a rather well-defined Raman signature assigned to the fully reduced $K_{0.78}V_2O_5$ bronze is observed, with 12 bands at 125, 211, 289, 361, 399, 445, 525, 555, 673, 730, 957 and 977 cm^{-1} .

To summarize, the main information gained by this Raman spectroscopy study are the following: (i) During the beginning of the discharge, K^+ ions are accommodated in γ' - V_2O_5 through a solid solution process involving only an increasing local disorder within the V_2O_5 layers of the formed K-poor γ - $K_xV_2O_5$ phase; (ii) A new K-rich phase coexisting with the K-poor γ - $K_xV_2O_5$ phase grows in the $0.35 \leq x \leq 0.63$ composition region. The slight discrepancy in the biphasic composition region as compared to XRD results can be easily understood because the high Raman scattering cross section of K-poor γ - $K_xV_2O_5$ delays the detection of the new $K_{0.5}V_2O_5$ phase; (iii) Raman spectra evolution in the $0.55 \leq x \leq 0.78$ domain points to a growing fingerprint of the K-rich phase, leading to a Raman signature assigned to the pure electroformed $K_{0.78}V_2O_5$ bronze.

3.3.2. Structural reversibility upon charge and further cycles.

Figure 8a compares the XRD patterns of a pristine electrode and those collected after a full cycle at C/20 and after 60 cycles at C/10. The XRD pattern after one discharge-charge cycle strongly resembles that achieved after discharge. This means that the oxidation process retains the structure of the electroformed bronze, the partial potassium extraction leading to the isostructural $K_{0.285}V_2O_5$ phase with following unit cell parameters: $a = 10.82$ (1) Å, $b = 3.68$ (1) Å and $c = 11.00$ (1) Å. The cell volume variation is negligible (438 Å^3 vs. 439 Å^3 for $K_{0.78}V_2O_5$), in line with the tiny unit cell parameter variations ($\Delta a/a = -0.7\%$, $\Delta b/b = -0.7\%$ and $\Delta c/c = +0.9\%$). A slight peak broadening is observed, that is related to a decrease by a factor 2 of the mean crystallite size on the first potassium extraction, (from 50 to ≈ 25 nm). After 60 cycles, no change is observed in the XRD pattern, which indicates the potassium bronze structure is retained, in line with the good cycling behaviour of the material (**Figure 4b**).

Further information on the structural evolution upon first charge and cycling can be drawn from Raman spectroscopy. The Raman spectra recorded after one and 60 discharge-charge cycles (**Figure 8b**) are characteristics of the K-poor γ - $K_xV_2O_5$ phase, with most of the typical bands of γ' - V_2O_5 , indicated by black spheres (at 138, 153, 267, 282, 389, 532, 694 and 1001 cm^{-1}). The slight band broadening and band shifts indicate a decrease of the grain size after one cycle, in good agreement with XRD observations showing a reduction by a factor 2 of the crystallite size. It is noteworthy that for both samples, none of the distinctive bands of the electroformed bronze can be detected, even in the high frequency region (see green dotted lines). This result interestingly confirms, as shown under quasi-thermodynamic experiments (**Figure S3**) that a complete potassium extraction from the $K_{0.78}V_2O_5$ bronze is possible and even occurs at 20°C in the outer shell of the particles ($\approx 100\text{-}300$ nm probed by Raman spectroscopy). The restauration of the typical Raman fingerprint of γ' - V_2O_5 points to the structural reversibility of the potassium insertion reaction in this polymorph.

The present XRD and Raman study establishes the first experimental evidence of structural changes upon potassium accommodation in γ' - V_2O_5 in the $4.4\text{ V} - 2.4\text{ V}$ potential range ($0 \leq x \leq 0.78$). The obtained results can be compared with a recent

study on the chemically prepared $K_{0.83}V_2O_5$ bronze that was studied at different states of charge-discharge in the $0.33 \leq x \leq 0.83$ range [27]. Depotassiation-potassiation was reported to occur as a solid solution region in the potassium bronze, as found in the present study from the first charge process and subsequent cycles. However, a thorough analysis of *ex situ* XRD experimental data from [27] was not performed. Instead the authors use DFT calculations to estimate the lattice parameters. Calculated values for a and b parameters were provided in the $0.125 \leq x \leq 0.875$ composition range. The in-plane a parameter was found to significantly decrease upon potassiation, from 11.55 Å to 10.93 Å (-5%), whereas our experimental data show a much softer decrease (-0.9%) (**Figure 6a**). Regarding the b parameter, DFT calculations predicted also a significant increase of 4.2% when x increases up to 0.875 [27], while the present experimental evidence show less marked variation ($+1.6\%$, see **Figure 6b**). Furthermore, as revealed by the present Raman study, the quantitative extraction process observed in the outer shell of the particles demonstrates the recovering of the “ γ' - V_2O_5 ” type arrangement upon full depotassiation. This experimental proof of structural reversibility calls into question DFT calculations from the same authors [27] predicting the

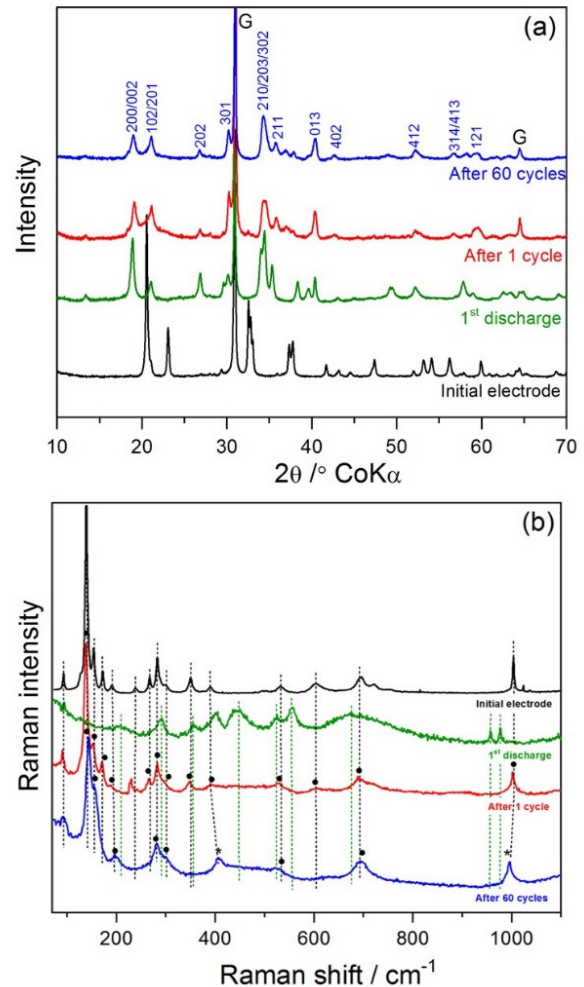


Figure 8. (a) X-Ray diffractions patterns and (b) Raman spectra of initial electrode, after 1st charge at C/20 and after 60 cycles at C/10. $4.4\text{ V} - 2.4\text{ V}$ voltage window.

charge product of $K_{0.83}V_2O_5$ would be a “ α - V_2O_5 ” type structure characterized by a much lower interlayer parameter value of 9.2 Å.

3.4. Structure of the electrochemically formed $K_{0.78}V_2O_5$ bronze. The formation of the $K_{0.78}V_2O_5$ bronze from electrochemical potassiation at room temperature of the γ - V_2O_5 oxide is reported here for the first time. We discuss in this section the structural peculiarities of this bronze, revealed by XRD and Raman spectroscopy (**Figure 9**). The refinement of the XRD pattern of the $K_{0.78}V_2O_5$ electrode (**Figure 9a**), leads to low R-factors ($R_p = 2.40\%$, $wR_p = 3.79\%$, $\chi^2 = 7.32$), which confirms the accuracy of the Rietveld refinement. The refined cell parameters, $a = 10.888(1)$ Å, $b = 3.7016(2)$ Å and $c = 10.8928(8)$ Å, are in good agreement with those calculated for the chemically synthesized $K_{0.83}V_2O_5$ phase [27].

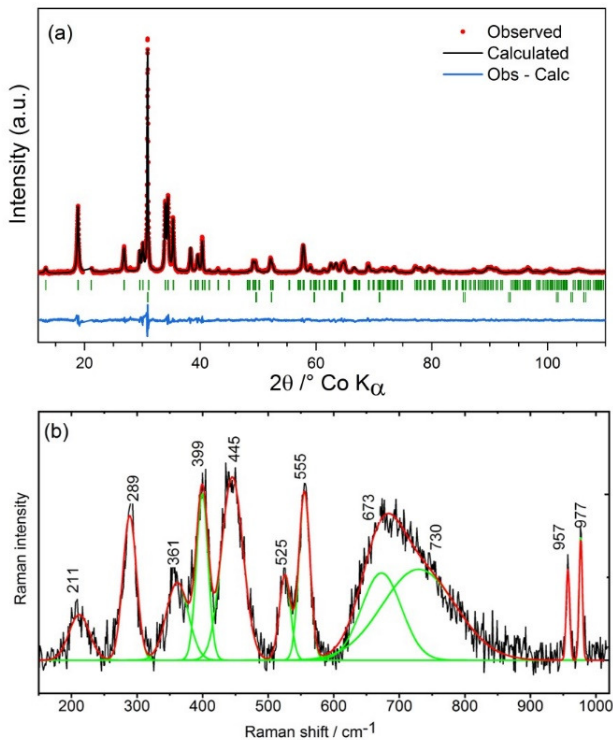


Figure 9. (a) Rietveld refinement of the X-Ray diffraction pattern of $K_{0.78}V_2O_5$. Upper marks correspond to the $K_{0.78}V_2O_5$ phase; Vertical bars in green represent the position of Bragg reflections. Lower marks figure the graphite contribution; (b) Raman spectrum of $K_{0.78}V_2O_5$ with the band deconvolution shown below (in green).

Table 3 gives the refined atomic positions and structural parameters deduced from the refinement of the XRD data. There are eight independent atomic positions; all of them in general Wyckoff positions $4a$. The crystal structure of $K_{0.78}V_2O_5$ based on these data is shown in **Figure 10**. This is a layered-like arrangement with infinite “ V_2O_5 ” layers running in the b and c directions and stacked along the a axis (**Figures 10a-b**), the potassium atoms being located in $4a$ sites between them, in nine fold coordination with oxygen atoms (**Figure 10c**). According to the literature, K^+ is observed in 12 different coordinations, from 4 to 15, with a preference for coordination numbers 9, 8 and 10 [53]. A detailed representation of the V_2O_5 layer in

$K_{0.78}V_2O_5$ (**Figure 10b**) shows that chains are made of VO_5 units linked in pairs along the c -axis by corner bridging O_3 oxygen, with apex O_1 oxygen atoms in same orientation, while edge-sharing VO_5 pyramids pairs are linked by ladder step $V-O_2$ bonds (indicated by dashed line) and point in opposite direction. In such a way, $K_{0.78}V_2O_5$ structure diverges from that of γ - V_2O_5 , characterized by edge-sharing VO_5 pyramids oriented alternatively up and down (see inset in **Figure 2b**) and shows similarities with the α - V_2O_5 layers’ arrangement made of equivalent VO_5 pyramids linked in pairs pointing alternatively up and down.

Atomic positions in $K_{0.78}V_2O_5$, listed in **Table 3**, lead to the $V-O$ and $K-O$ bond lengths gathered in **Table 4**. The $K-O$ bond lengths, in the range 2.8–3 Å, are in good agreement with the mean values observed in the literature data [53]. $V-O$ bond lengths in γ - V_2O_5 obtained from the Rietveld refinement (**Fig. S1**) are also displayed in **Table 4** for comparison. Analyzing the particular characteristics of γ - V_2O_5 and $K_{0.78}V_2O_5$ lattices (**Table 4**), one can distinguish the structural changes induced by potassium intercalation at the scale of the chemical bond. They can be summarized as follows: (i) the apical V_a-O_{1a} and V_b-O_{1b} bonds markedly lengthen (by 2.5 % and 5%, respectively, in line with the expansion of the interlayer unit cell parameter (see **Table 2**); (ii) the V_a-O_3 and V_b-O_3 bonds forming the $V_a-O_3-V_b$ bridge lengthen by 2-3% but remain symmetric; (iii) the length of the V_b-O_{2b} bond increases significantly (+5.8%) while the V_a-O_{2a} bond remains almost unchanged (+0.2%); (iv) the ladder step (V_a-O_{2b})_{LS} shortens (-2.4%); (v) the $V_a-O_3-V_b$ bridge angle increases, from 123 to 140°. This noticeable increase in the angle value of the $V-O_3-V$ bond linking the two corner-sharing VO_5 pyramids reflects the peculiar layer unfolding induced upon potassium insertion in γ - V_2O_5 . The corresponding value of 123.4° in γ - V_2O_5 highlights the significant puckering of the layers compared to the quasi-smooth α - V_2O_5 polymorph for which this angle is $\approx 148^\circ$ [54].

Table S1 gathers the atomic structural features of γ - V_2O_5 and γ -Li(Na) V_2O_5 bronzes. It is noteworthy to compare the effect of Li, Na and K insertion in γ - V_2O_5 on the value of this specific angle. While Li insertion does not modify the layers’ puckering, Na and especially K insertion produce the reverse trend, as illustrated by the angle increase that reaches 127° for the Na bronze and 140° for the potassiated phase (**Figure 10b**), i. e. a value very close to that observed for α - V_2O_5 . Such effect arises probably from the higher polarizability of K^+ ions [51] as compared to Na and Li. Owing to the similar lattice constitution (V_2O_5 chains linked by ladder step (V_a-O_{2b})_{LS} and (V_b-O_{2a})_{LS} contact linkages and stacked perpendicular to the layers), the $K_{0.78}V_2O_5$ Raman spectrum (**Figure 9b**) should present some analogy with those previously reported for layered $M_xV_2O_5$ -based structures ($M = Li, Na$) [39, 45, 46, 55–57]. Indeed, **Table S1** shows that $V-O$ bond lengths for $K_{0.78}V_2O_5$ and those previously reported for γ -Li(Na) V_2O_5 lattices lie in the same range (1.5 – 2.1 Å). As a direct consequence, the Raman spectra of these three alkali-intercalated compounds exhibit analogous general shape (see **Figure S7**), with several band shifts reflecting the influence of the inserted alkali specie at the scale of the chemical bond. Such similarity allows us to propose a consistent assignment of the $K_{0.78}V_2O_5$ Raman spectrum (see **Table 5**), by relying on our previous vibrational dynamics analysis

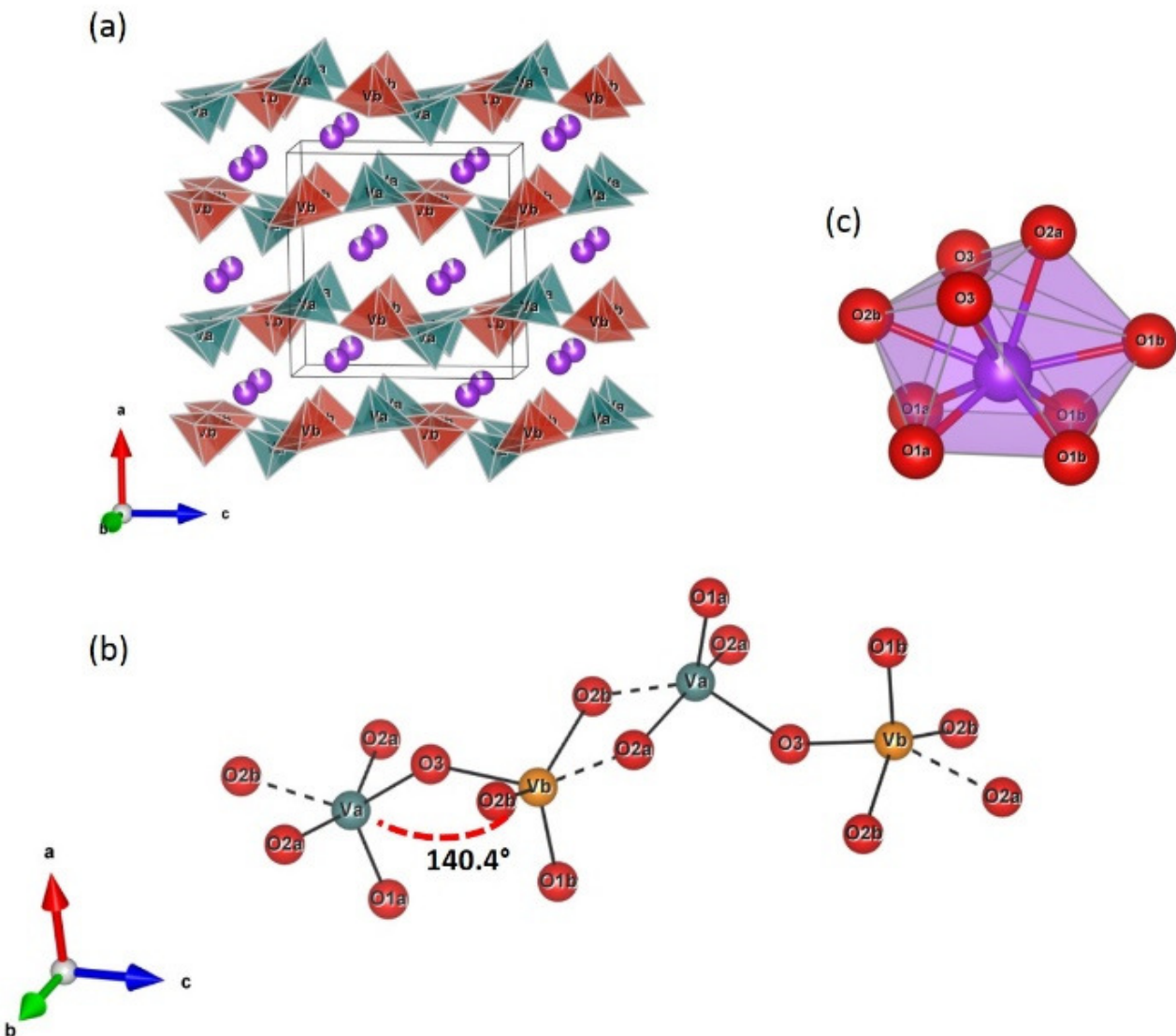


Figure 10. (a) Structure of $K_{0.78}V_2O_5$ phase. Violet spheres represent K atoms in their crystallographic sites. V_aO_5 and V_bO_5 square pyramids are shown in blue and red color, respectively. (b) Local structure of the V_2O_5 layers showing the two vanadium environments. Dashed lines indicate ladder-step V–O bonds; The $V_aO_3V_b$ bond angle of 140.4° is indicated by a dashed curve (c) Local coordination of the potassium atom.

performed on V_2O_5 polymorphs [45, 46] and γ -Li(Na) V_2O_5 bronzes [39, 55–57]. The two highest-frequency bands at 977 and 957 cm^{-1} correspond to the stretching vibrations of the short apical $V=O_1$ bonds. The lower wavenumber in $K_{0.78}V_2O_5$ is in good agreement with the longer vanadyl bond as compared to the Na-bronze (**Table S1**). The broad peak at 730 cm^{-1} is partly assigned to the stretching vibration localized within the $V_a-O_{2a}-V_a$ bridge. The corresponding $\nu(V_b-O_{2b}-V_b)_S$ stretching mode along the b -axis is shifted at lower frequency of 445 cm^{-1} due to the significant lengthening of the V_b-O_{2b} bond on potassium insertion. Owing to the increase in V_a-O_3 and V_b-O_3 bond lengths upon potassium insertion, both asymmetric and symmetric $\nu(V_a-O_3-V_b)$ stretching modes involving the motion of the O_3 bridging oxygen along the c -axis are seen at lower frequencies (730 and 555 cm^{-1} , respectively) as compared to γ - V_2O_5 (752 and 603 cm^{-1} , respectively). Modes involving the longer ladder step

bonds (indicated by dashed lines in **Figure 10b**) are usually observed at lower frequency (around 500 - 550 cm^{-1} , see **Table 5**). In the K-bronze, the corresponding $\nu(V_b-O_{2a})_{LS}$ and $\nu(V_a-O_{2b})_{LS}$ vibrations are likely to occur at 525 and 673 cm^{-1} , respectively, the higher frequency of the latter coming from the unusually short length of the $(V_a-O_{2b})_{LS}$ bond. Finally, peaks below 400 cm^{-1} have been previously assigned to the complex distortions of the V_2O_4 ladders in V_2O_5 -based compounds [45, 46, 55]. DFT calculations on the vibrational dynamics of $K_{0.78}V_2O_5$ are in progress and should shed further light on these new Raman data.

The valence states of the vanadium ions have been estimated using the bond valence sum (BVS) method [58, 59] (**Table 4**). The obtained values point to different oxidation states between the two inequivalent vanadium sites. Indeed, V_a site is filled by V^{+5} ions (BVS value = 4.99) while V_b site accommodates V^{+4}

species (BVS value = 3.89). This result reveals a localized character of electron, comparable to that also observed in vanadium bronzes with γ -type puckered layer structure such as γ -LiV₂O₅ [54] and γ -Na_{0.96}V₂O₅ [39, 56] and suggests that the V_b site is the redox center. However, the charge distribution in the present potassium bronze differs, since a strict alternation between V⁺⁵ and V⁺⁴ ions along the in-plane *c*-axis is observed (**Figure 10a**) while for γ -type structure, V⁺⁵ or V⁺⁴ are linked in pairs [39, 55, 56]. This peculiarity should favor electron conduction within the V₂O₅ layers of the potassium bronze. Finally it should be noted the high electron localization in K_{0.78}V₂O₅ contrasts with the average valence of V^{+4.5} observed for the α' -NaV₂O₅ bronze in which vanadium ions occupy a single site [52].

4. CONCLUSIONS

In this work, the structural and electrochemical properties of the γ -V₂O₅ polymorph toward potassium insertion are reported for the first time. We show that in spite of its large size, a high amount of potassium (up to 0.9 K⁺ mol⁻¹ in the 4.4 V – 1.5 V voltage window) can be electrochemically accommodated between the puckered layers of γ -V₂O₅ at a high energy level of 3.3 V vs K^{+/K}, i. e. very close to that reported for Li⁺ and Na⁺ intercalation. These promising potassium insertion properties clearly overcome those exhibited by the conventional α -V₂O₅ polymorph, characterized by a very low working potential of 1.5 V vs K^{+/K}. The structural study of the potassiation-depotassiation mechanism in γ -V₂O₅ in the 4.4 V – 2.4 V voltage range reveals a peculiar structure rearrangement upon the first electrochemical potassiation corresponding to the formation of a new layered K_xV₂O₅ system. The K_{0.5}V₂O₅ phase is shown to coexist with γ -V₂O₅ in the 0.05 ≤ *x* < 0.55 region, then becomes enriched with potassium up to the K_{0.78}V₂O₅ composition. A detailed description of the fully reduced K_{0.78}V₂O₅ structure is provided at both the long-range order and atomic scale. It crystallizes in the *Pnma* space group (*a* = 10.89 Å, *b* = 3.70 Å, *c* = 10.89 Å) and exhibits a moderate interlayer expansion limited to 9.4% upon potassium insertion in γ -V₂O₅ (vs. 18% in the case of sodiation), but a significant unfolding of the layers that probably compensates the volume expansion. In K_{0.78}V₂O₅, V₂O₅ layers are composed of VO₅ pairs pointing alternatively up and down in the interlayer spacing, which differs from the alternation of single VO₅ pyramids in γ -V₂O₅. Such change illustrates the peculiar ability of the pristine γ -V₂O₅ host lattice to minimize the structural changes upon K⁺ accommodation. The electrochemical study shows that potassium ions are mobile within the K_{0.78}V₂O₅ structure, 0.5 K⁺ mol⁻¹ being extracted at C/10 at an average potential of 3.3 V vs. K^{+/K}. Upon further cycling, reversible K⁺ exchange occurs in the K_xV₂O₅ system (0.3 ≤ *x* ≤ 0.7), by involving only a slight structural breathing and allowing a capacity value of 48 mAh g⁻¹ stabilized over at least 100 cycles. This study highlights that K_{0.78}V₂O₅ is a new and unique structure among the V₂O₅ polymorphs and V₂O₅-derived materials, which confirms once more the richness of polymorphism of the V₂O₅-based phases in terms of structural variety and electrochemical behaviour. Further optimization in progress should allow to fully benefiting from the advantages provided by this new electroformed potassium host structure: a high operational potential, a high amount of accommodated K⁺ ion and a remarkable stability upon cycling.

ASSOCIATED CONTENT

Supporting Information.

This material is available free of charge via the Internet at <http://pubs.acs.org>. Local atomic environment in γ -V₂O₅ and M_xV₂O₅ bronzes (M = Li, Na, K), Rietveld refinement of γ -V₂O₅ X-ray diffraction pattern, First discharge/charge cycle of γ -V₂O₅ at 20°C at C/10 rate in Li and Na-based electrolytes, First discharge-charge cycle of γ -V₂O₅ at C/60, at 20°C and 50°C in K-based electrolyte, Electrochemical performance of γ -V₂O₅ at 20°C in the enlarged 4.4 V – 1.5 V voltage window in K-based electrolyte, Electrochemical performance of α -V₂O₅ at 20°C in K-based electrolyte, Schematic representation of the proposed intermediate K_xV₂O₅ phase, Raman spectra of γ -LiV₂O₅, γ -Na_{0.96}V₂O₅ and K_{0.78}V₂O₅.

Author Contributions

The manuscript was written through contributions of all authors. / All authors have given approval to the final version of the manuscript. /

Funding Sources

French ANR project “CASSIOPES” N°17-CE09-0016-03.

Notes

The authors declare that they have no known competing financial interests or personal relationships that could have appeared to influence the work reported in this paper.

ACKNOWLEDGMENT

One of the authors wishes to thank the French ANR project “CASSIOPES” N°17-CE09-0016-03 for their financial support. All the authors would like to thank Rémy Pires Brazuna (ICMPE-CNRS) for his valuable contribution in SEM-EDS analysis.

TABLES

Electrode history	x in $K_xV_2O_5$ (EC)	K/V (EC)	K/V (EDS)
Discharged to 2.4 V	0.78	0.39	0.41
Discharged to 1.5 V	0.89	0.445	0.464
After 1 cycle (4.4 V – 2.4 V)	0.285	0.143	0.139
After 1 cycle (4.4 V – 1.5 V)	0.32	0.16	0.164

Table 1. K/V ratios in electrodes from EDS analysis and electrochemistry (EC).

Phase (<i>Pnma</i>)	<i>In-</i> <i>plane</i> (Å)	<i>In-</i> <i>plane</i> <i>b</i> (Å)	<i>Inter-</i> <i>layer</i> (Å)	<i>Unit cell</i> <i>volume</i> (Å ³)	<i>Molar</i> <i>volume</i> (cm ³ mol ⁻¹)
γ'-V ₂ O ₅	9.95	3.59	10.04	358	54
γ-LiV ₂ O ₅	9.69	3.61	10.68	373	56
γ-Na _{0.96} V ₂ O ₅	9.78	3.63	11.89	422	63
K _{0.78} V ₂ O ₅	10.89	3.70	10.89	439	66

Table 2. Unit cell parameters, unit cell volumes and molar volumes of γ'-V₂O₅ and electroformed Me_xV₂O₅ bronzes (Me = Li [34], Na [39], K [this work]).

Atom type (la- bel)	Wyckoff position	x	y	z	U _{iso} (Å ²)
K (K)	4 <i>a</i>	0.0610 (4)	0.75	0.1903 (6)	0.026 (2)
V (V _a)	4 <i>a</i>	0.6644 (4)	0.75	0.9061 (6)	0.017 (1)
V (V _b)	4 <i>a</i>	0.7315 (3)	0.75	0.5964 (5)	0.017 (1)
O (O _{2a})	4 <i>a</i>	0.692 (1)	0.25	0.932 (1)	0.008 (2)
O (O _{2b})	4 <i>a</i>	0.7958 (8)	0.25	0.578 (2)	0.008 (2)
O (O _{1a})	4 <i>a</i>	0.523 (1)	0.75	0.865 (1)	0.008 (2)
O (O _{1b})	4 <i>a</i>	0.580 (1)	0.75	0.585 (1)	0.008 (2)
O (O ₃)	4 <i>a</i>	0.753 (1)	0.75	0.766 (2)	0.008 (2)
Space group <i>Pnma</i> ; <i>a</i> = 10.888 (1) Å, <i>b</i> = 3.7016 (2) Å and <i>c</i> = 10.8928 (8) Å $\alpha = \beta = \gamma = 90^\circ$; <i>V</i> = 439.03 Å ³ ; <i>Z</i> = 4 <i>R_p</i> = 2.40 %, <i>wR_p</i> = 3.79 %, χ^2 = 7.32; Number of refined parameters: 52					

Table 3. Wyckoff positions, fractional atomic coordinates and isotropic displacement parameters for electroformed extracted from the Rietveld refinement of electrochemically formed K_{0.78}V₂O₅.

	γ' -V ₂ O ₅	K _{0.78} V ₂ O ₅
V _a -O _{1a}	1.560	1.602 (13)
V _a -O ₃	1.749	1.809 (13)
V _a -O _{2a} (x2)	1.893	1.898 (4)
(V _a -O _{2b}) _{LS}	1.968 (V _a -O _{2a}) _{LS}	1.921 (18)
Volume of V _a O ₅	4.461	4.87
BVS (V _a)	+5.29	+4.99
V _b -O _{1b}	1.576	1.655 (10)
V _b -O ₃	1.827	1.860 (20)
V _b -O _{2b} (x2)	1.880	1.989 (4)
(V _b -O _{2a}) _{LS}	2.028 (V _b -O _{2b}) _{LS}	1.968 (17)
Volume of V _b O ₅	4.531	5.29
BVS (V _b)	+4.99	+3.89
$\widehat{V_aO_3V_b}$	123°4	140.4°
V _b -O ₃ / V _a -O ₃	1.04	1.03

K-O _{1a}	3.01(1)
K-O _{1a} (x2)	3.01(1)
K-O _{1b} (x2)	2.81(1)
K-O _{2b}	3.00(1)
K-O ₃ (x2)	2.78(1)
K-O _{2a}	2.96(2)

Table 4. V–O bond lengths (in Å) in γ' -V₂O₅; V–O and K–O bond lengths (in Å) in K_{0.78}V₂O₅; V_aO₃V_b bond angle; V_a and V_b valence states estimated using the BVS approximation; VO₅ pyramid volumes (in Å³). Atoms labels correspond to those shown in inset of Figs. 2b and Fig. 10b. LS: ladder step bonds (shown by dashed lined in Figs. 2b and Fig. 10b).

$K_{0.78}V_2O_5$ [This work]		$\gamma\text{-Na}_{0.96}V_2O_5$ [39]	$\gamma\text{-LiV}_2O_5$ [54]		$\gamma'\text{-V}_2O_5$ [45, 46]	
Raman peak (cm^{-1})	Assignment	Raman peak (cm^{-1})	Raman peak (cm^{-1})	Assignment	Raman peak (cm^{-1})	Assignment
977 957	$\nu(V=O_1)$	1005 959	987 965	$\nu(V=O_1)$	1021, 1037 1003	$\nu(V=O_1)$
730	$\nu_{as}(V_a-O_3-V_b)$ $\nu(V_a-O_{2a}-V_a)$	717	737	$\nu(V_a-O_3) +$ $\nu_{as}(V_a-O_{2a}-V_a)$	752	$\nu_{as}(V_a-O_3-V_b)$
					722	$\nu(V_a-O_{2a}-V_a)$
					603	$\nu_s(V_a-O_3-V_b)$
673	$\nu(V_a-O_{2b})_{LS}$	655	646	$\nu_{as}(V_b-O_{2b}-V_b)$	694	$\nu(V_b-O_{2b}-V_b)$
555	$\nu_s(V_a-O_3-V_b)$	546	549	$\nu(V_a-O_{2a})_{LS}$	532	$\nu(V_a-O_{2a})_{LS}$
525	$\nu(V_b-O_{2a})_{LS}$		533	$\nu(V_b-O_{2b})_{LS}$	500	$\nu(V_b-O_{2b})_{LS}$
445	$\nu(V_b-O_{2b}-V_b)$	470	462	$\nu(V_b-O_3)$		
399, 261 289, 208	LM (V_a, V_b)	388, 323, 297, 250, 191, 221, 155	369, 329, 272, 253, 205, 171	LM (V_a, V_b)	390, 349, 299, 282, 266, 238, 190, 171, 138	LM (V_a, V_b)
125	Rot (V_a, V_b)	110, 85	124, 100	Rot (V_a, V_b)	126, 153, 92	Rot (V_a, V_b)

Table 5. Positions of Raman peaks in the Raman spectra of $\gamma'\text{-V}_2O_5$, $\gamma\text{-LiV}_2O_5$, $\gamma\text{-Na}_{0.96}V_2O_5$ and $K_{0.78}V_2O_5$ with their assignments. LM: ladder modes; LS: ladder step bonds. Atoms labels correspond to those shown in inset of Fig. 2b and Fig. 10b.

REFERENCES

- (1) Yabuuchi, N.; Kubota, K.; Dahbi, M.; Komaba, S. Research developments on sodium-ion batteries. *Chem. Rev.* **2014**, *114*, 11636–11682.
- (2) Kim H.; Kim, J. C.; Bianchini, M.; Seo, D.-H.; Rodriguez-Garcia, J.; Ceder, G. Recent progress and perspective in electrode materials for K-ion batteries. *Adv. Energy Mater.* **2017**, *8*, 1702384.
- (3) Hosaka, T.; Kubota, K.; Shahul Hameed, A.; Komaba, S. Research development on K-ion batteries. *Chem. Rev.* **2020**, *120*, 6358–6466.
- (4) Bie, X.; Kubota, K.; Hosaka, T.; Chihara, K.; Komaba, S. A novel K-ion battery: hexacyanoferrate(II)/Graphite cell. *J. Mater. Chem. A* **2017**, *5*, 4325–4330.
- (5) Chihara, K.; Katogi, A.; Kubota, K.; Komaba, S. KVPO₄F and KVOPO₄ toward 4V-class potassium-ion batteries. *Chem. Commun.* **2017**, *53*, 5208–5211.
- (6) Kim, H.; Seo, D.-H.; Bianchini, M.; Clément, R. J.; Kim, H.; Kim, J. C.; Tian, Y.; Shi, T.; Yoon, W.-S.; Ceder, G. A new strategy for high voltage cathodes for K-ion batteries: Stoichiometric KVPO₄F. *Adv. Energy Mater.* **2018**, *8*, 1801591.
- (7) Hosaka, T.; Kubota, K.; Kojima, H.; Komaba, S. Highly concentrated electrolyte solutions for 4 V class potassium-ion batteries. *Chem. Commun.* **2018**, *54*, 8387–8390.
- (8) Eftekhari, A. Potassium secondary cell based on Prussian blue cathode. *J. Power Sources* **2004**, *126*, 221–228.
- (9) Jiang, X.; Zhang, T.; Yang, L.; Li, G.; Lee, J. Y. A Fe/Mn-Based Prussian Blue Analogue as a K-Rich Cathode Material for Potassium-Ion Batteries. *ChemElectroChem* **2017**, *4*, 2237–2242.
- (10) Hironaka, Y.; Kubota, K.; S. Komaba, K. P2 and P3-K_xCoO₂ as an electrochemical potassium intercalation host. *Chem. Commun.* **2017**, *53*, 3693–3696.
- (11) Kim, H.; Kim, J. C.; Bo, S. H.; Shi, T.; Kwon, D. H.; Ceder, G. K-ion batteries based on a P2 type K_{0.6}CoO₂. *Adv. Energy Mater.* **2017**, *7*, 1700098.
- (12) Vaalma, C.; Giffin, G. A.; Buchholz, D.; Passerini, S. Non-Aqueous K-Ion Battery Based on Layered K_{0.3}MnO₂ and Hard Carbon/Carbon Black. *J. Electrochem. Soc.* **2016**, *163*, A1295–A1299.
- (13) Liu, C. L.; Luo, S. H.; Huang, H. B.; Zhai, Y. C.; Wang, Z. W. Layered potassium-deficient P2- and P3-type cathode materials K_xMnO₂ for K-ion batteries. *Chem. Engineer. J.* **2019**, *356*, 53–59.
- (14) H. Kim, D. H. Seo, J. C. Kim, S. H. Bo, L. Liu, T. Shi, G. Ceder, Investigation of potassium storage in layered P3-type K_{0.5}MnO₂ cathode. *Adv. Mater.* **2017**, *29*, 1702480.
- (15) X. Wang, X. Xu, C. Niu, J. Meng, M. Huang, X. Liu, Z. Liu, L. Mai, Earth abundant Fe/Mn-based layered oxide interconnected nanowires for advanced K-ion full batteries. *Nano Lett.* **2017**, *17*, 544–550.
- (16) C. L. Liu, S. H. Luo, H. B. Huang, Y. C. Zhai, Z. W. Wang, Low-cost layered K_{0.45}Mn_{0.9}Mg_{0.1}O₂ as a high performance cathode material for K-ion battery. *ChemElectroChem.* **2019**, *6*, 2308–2315.
- (17) M. Y. Cho, J. Y. Jo, J. U. Choi, S. T. Myung, Cycling stability of layered potassium manganese oxide in nonaqueous potassium cells. *ACS Applied Mater. Interfaces* **2019**, *11*, 27770–27779.
- (18) P. Bai, K. Jiang, X. Zhang, J. Xu, S. Guo, H. Zhou, Ni-Doped Layered Manganese Oxide as a Stable Cathode for Potassium-Ion Batteries. *ACS Appl. Mater. Interfaces* **2020**, *12*, 10490–10495.
- (19) J. U. Choi, J. Kim, J.-Y. Hwang, J. H. Jo, Y.-K. Sun, S. T. Myung, K_{0.54}Co_{0.5}Mn_{0.5}O₂: new cathode with high power capability for potassium-ion batteries. *Nano Energy* **2019**, *61*, 284–294.
- (20) Rastgoo-Deylami, M.; Heo, J. W.; Hong, S.-T. High potassium storage capability of H₂V₃O₈ in a non-aqueous electrolyte. *ChemistrySelect* **2019**, *4*, 11711–11717.
- (21) Tian, B.; Tang, W.; Su, C.; Li, Y. Reticular V₂O₅·0.6H₂O xerogel as cathode for rechargeable potassium-ion batteries. *ACS Appl. Mater. Interfaces* **2018**, *10*, 642–650.
- (22) Liu, X.; Elia, G. A.; Gao, X.; Qin, B.; Zhang, H.; Passerini, S. Highly concentrated KTFSL: glyme electrolytes for K/bilayered-V₂O₅ batteries. *Batteries and Supercaps.* **2020**, *3*, 261–267.
- (23) Xu, Y.; Dong, H.; Zhou, M.; Zhang, C.; Wu, Y.; Li, W.; Dong, Y.; Lei, Y. Ammonium vanadium as a potassium-ion battery cathode with high rate capability and cyclability. *Small Methods* **2019**, *3*, 1800349.
- (24) Clites, M.; Hart, J. L.; Taheri, M. L.; Pomerantseva, E. Chemically preintercalated bilayered K_xV₂O₅·nH₂O nanobelts as a high-performing cathode material for K-ion batteries. *ACS Energy Lett.* **2018**, *3*, 562–567.
- (25) Deng, L.; Niu, X.; Ma, G.; Yang, Z.; Zeng, L.; Zhu, Y.; Guo, L. Layered potassium vanadate K_{0.5}V₂O₅ as a cathode material for nonaqueous potassium ion batteries. *Adv. Funct. Mater.* **2018**, *28*, 1800670.
- (26) Zhu, Y.-H.; Zhang, Q.; Yang, X.; Zhao, E.-Y.; Sun, T.; Zhang, X.-B.; Wang, S.; Yu, X.-Q.; Yan, J.-M.; Jiang, Q. Reconstructed orthorhombic V₂O₅ polyhedra for fast ion diffusion in K-ion batteries. *Chem* **2019**, *5*, 168–179.
- (27) Zhang, Y.; Niu, X.; Tan, L.; Deng, L.; Jin, S.; Zeng, L.; Xu, H.; Zhu, Y. K_{0.83}V₂O₅: a new layered compound as a stable cathode material for potassium-ion batteries. *ACS Appl. Mater. Interfaces* **2020**, *12*, 9332–9340.
- (28) Pereira-Ramos, J.-P.; Messina, R.; Perichon, J. Electrochemical formation of vanadium pentoxide bronzes M_xV₂O₅ in molten dimethylsulfone. *J. Electrochem. Soc.* **1988**, *135*, 3050–3057.
- (29) Ye, F.; Lu, D.; Gui, X.; Wang, T.; Zhuang, X.; Luo, W.; Huang, Y. Atomic layer deposition of core-shell structured V₂O₅@CNT sponge as cathode for potassium ion batteries. *J. Materiomics* **2019**, *5*, 344–349.
- (30) Vishnuprakash, P.; Nithya, C.; Premalatha, M. Exploration of V₂O₅ nanorod@rGO heterostructure as potential cathode material for potassium-ion batteries. *Electrochim. Acta* **2019**, *309*, 234–241.
- (31) Parija, A.; Prendergast, D.; Banerjee, S. Evaluation of multivalent cation insertion in single- and double-layered polymorphs of V₂O₅. *ACS Appl. Mater. Interfaces* **2017**, *9*, 23756–23765.
- (32) Parija, A.; Liang, Y.; Andrews, J. L.; De Jesus, L. R.; Prendergast, D.; Banerjee, S. Topochemically de-intercalated phases of V₂O₅ as cathode materials or multivalent intercalation batteries: a first principle evaluation. *Chem. Mater.* **2016**, *28*, 5611–5620.
- (33) Cocciantelli, J. M.; Doumerc, J. P.; Pouchard, M.; Broussely, M.; Labat, J. Crystal-chemistry of electrochemically inserted Li_xV₂O₅. *J. Power Sources* **1991**, *34*, 103–111.
- (34) Baddour-Hadjean, R.; Safrany Renard, M.; Pereira-Ramos, J.-P. Unraveling the structural mechanism of Li insertion in γ'-V₂O₅ and its effect on cycling properties. *Acta Mater.* **2019**, *165*, 183–191.
- (35) Baddour-Hadjean, R.; Safrany Renard, M.; Pereira-Ramos, J.-P. Kinetic insight into the electrochemical lithium insertion process in the puckered-layer γ'-V₂O₅ polymorph. *J. Electrochem. Soc.* **2019**, *166*, A1–A6.
- (36) Safrany Renard, M.; Emery, N.; Baddour-Hadjean, R.; Pereira-Ramos, J.-P. γ'-V₂O₅: A new high voltage cathode material for sodium-ion battery. *Electrochim. Acta* **2017**, *252*, 4–11.
- (37) Safrany Renard, M.; Baddour-Hadjean, R.; Pereira-Ramos, J.-P. Kinetic insight into the electrochemical sodium insertion-extraction mechanism of the puckered γ'-V₂O₅ polymorph. *Electrochim. Acta* **2019**, *322*, 134670.
- (38) Baddour-Hadjean, R.; Safrany Renard, M.; Pereira-Ramos, J.-P. Enhanced electrochemical properties of ball-milled γ'-V₂O₅ as cathode material for Na-ion batteries: a structural and kinetic investigation. *J. Power Sources* **2021**, *482*, 229017.
- (39) Emery, N.; Baddour-Hadjean, R.; Batorybekuly, D.; Laïk, B.; Bakenov, Z.; Pereira-Ramos, J.-P. γ-Na_{0.96}V₂O₅: a new competitive cathode material for sodium ion battery synthesized by a soft chemistry route. *Chem. Mater.* **2018**, *30*, 5305–5314.
- (40) Muller, D.; Baddour-Hadjean, R.; Tanabe, M.; Huynh, L. T. N.; Le, L. M. P.; Pereira-Ramos, J.-P. Electrochemically formed α'-NaV₂O₅: a new sodium intercalation compound. *Electrochim. Acta* **2015**, *176*, 586–593.

(41) Baddour-Hadjean, R.; Huynh, L.T. N.; Emery, N.; Pereira-Ramos, J.-P. The richness of V_2O_5 polymorphs as superior cathode materials for sodium insertion. *Electrochim. Acta* **2018**, *270*, 129–137.

(42) Mjejri, I.; Rougier, A.; Gaudon, M. Low-cost and facile synthesis of the vanadium oxides V_2O_3 , VO_2 , and V_2O_5 and their magnetic, thermochromic and electrochromic properties. *Inorg. Chem.* **2017**, *56*, 1734–1741.

(43) Larson, A. C.; Von, R. B.; Lansce, D. General Structure Analysis System (GSAS), Los Alamos National Laboratory, Technical Report N° LAUR86-748, 2004.

(44) Toby, B. H. EXPGUI, a graphical user interface for GSAS. *J. Appl. Crystallogr.* **2001**, *34*, 210–213.

(45) Baddour-Hadjean, R.; Smirnov, M. B.; Kazimirov, V. Y.; Smirnov, K. S.; Pereira-Ramos, J.-P. The Raman spectrum of the γ - V_2O_5 polymorph: A combined experimental and DFT study. *J. Raman Spectrosc.* **2015**, *46*, 406–412.

(46) Smirnov, M. B.; Roginskii, E. M.; Smirnov, K. S.; Baddour-Hadjean, R.; Pereira-Ramos, J.-P. Unraveling the structure–Raman spectra relationships in V_2O_5 polymorphs via a comprehensive experimental and DFT study. *Inorg. Chem.* **2018**, *57*, 9190–9204.

(47) Kim, H.; Tian, Y.; Ceder, G. Origin of capacity degradation of high voltage $KVPO_4F$ cathode. *J. Electrochem. Soc.* **2020**, *167*, 110555.

(48) Han, J.; Li, G.-N.; Liu, F.; Wang, M.; Zhang, Y.; Hu, L.; Dai, C.; Xu, M. Investigation of $K_3V_2(PO_4)_3/C$ nanocomposite as high potential cathode materials for potassium-ion batteries. *Chem. Commun.* **2017**, *53*, 1805–1808.

(49) Lin, X.; Huang, J.; Tan, H.; Huang, J.; Zhang, B. $K_3V_2(PO_4)_2F_3$ as a robust cathode for potassium-ion batteries. *Energy Storage Mater.* **2019**, *16*, 97–101.

(50) Shannon, R. D. Revised effective ionic radii and systematic studies of interatomic distances in halides and chalcogenides. *Acta Crystallogr. A* **1976**, *32*, 751–767.

(51) Tessman, J. R.; Kahn, A. H.; Shockley, W. Electronic polarizabilities of ions in crystals. *Phys. Rev.* **1953**, *92*, 890–895.

(52) Baddour-Hadjean, R.; Huynh, L.T.N.; Emery, N.; Pereira-Ramos, J.-P. Lithium insertion in α' - NaV_2O_5 : Na-pillaring effect on the structural and electrochemical properties. *Electrochim. Acta* **2018**, *270*, 224–235.

(53) Gagné, O. C.; Hawthorne, F. Ch. Bond length distributions for ions bonded to oxygen: alkali and alkaline-earth metals. *Acta Crystallogr. Sect. B* **2016**, *72*, 602–625.

(54) Smirnov, M. B.; Kazimirov, V. Y.; Baddour-Hadjean, R.; Smirnov, K. S.; Pereira-Ramos, J.-P. Atomistic mechanism of phase transition in vanadium pentoxide. *J. Phys. Chem. Solids* **2014**, *75*, 115–122.

(55) Smirnov, M. B.; Roginskii, E. M.; Kazimirov, V. Y.; Smirnov, K. S.; Baddour-Hadjean, R.; Pereira-Ramos, J.-P.; Zhandun, V. S. Spectroscopic and computational study of structural changes in LiV_2O_5 cathodic material induced by lithium intercalation. *J. Phys. Chem. C* **2015**, *119*, 20801–20809.

(56) Safrany Renard, M.; Emery, N.; Roginskii, E. M.; Baddour-Hadjean, R.; Pereira-Ramos, J.-P. Crystal structure determination of a new sodium vanadium bronze electrochemically formed. *J. Solid State Chem.* **2017**, *254*, 62–68.

(57) Roginskii, E. M. M. B. Smirnov, K. S. Smirnov, R. Baddour-Hadjean, J. P. Pereira-Ramos, A. N. Smirnov, V. Yu. Davydov, A computational and spectroscopic study of the electronic structure of V_2O_5 -based cathode materials. *J. Phys. Chem. C* **2021**, *125*, 5848–5858.

(58) Brown, I. D. Recent developments in the methods and applications of the bond valence model. *Chem. Rev.* **2009**, *109*, 6858–6919.

(59) Brown, I. D.; Altermatt, D. Bond-valence parameters obtained from a systematic analysis of the inorganic crystal structure database. *Acta Crystallogr. Sect. B* **1985**, *41*, 244–247.

SYNOPSIS TOC.

